QUEEN: QUantized Efficient ENcoding for Streaming Free-viewpoint Videos

Sharath Girish[*]
University of Maryland
sgirish@cs.umd.edu

Tianye Li[†]
NVIDIA
tianyel@nvidia.com

Amrita Mazumdar[†]
NVIDIA
amritam@nvidia.com

Abhinav Shrivastava
University of Maryland
abhinav@cs.umd.edu

David Luebke
NVIDIA
dluebke@nvidia.com

Shalini De Mello
NVIDIA
shalinig@nvidia.com

Abstract

Online free-viewpoint video (FVV) streaming is a challenging problem, which is relatively under-explored. It requires incremental on-the-fly updates to a volumetric representation, fast training and rendering to satisfy real-time constraints and a small memory footprint for efficient transmission. If achieved, it can enhance user experience by enabling novel applications, *e.g.*, 3D video conferencing and live volumetric video broadcast, among others. In this work, we propose a novel framework for QUantized and Efficient ENcoding (QUEEN) for streaming FVV using 3D Gaussian Splatting (3D-GS). QUEEN directly learns Gaussian attribute residuals between consecutive frames at each time-step without imposing any structural constraints on them, allowing for high quality reconstruction and generalizability. To efficiently store the residuals, we further propose a quantization-sparsity framework, which contains a learned latent-decoder for effectively quantizing attribute residuals other than Gaussian positions and a learned gating module to sparsify position residuals. We propose to use the Gaussian viewspace gradient difference vector as a signal to separate the static and dynamic content of the scene. It acts as a guide for effective sparsity learning and speeds up training. On diverse FVV benchmarks, QUEEN outperforms the state-of-the-art online FVV methods on all metrics. Notably, for several highly dynamic scenes, it reduces the model size to just 0.7 MB per frame while training in under 5 sec and rendering at $\sim$350 FPS.

1 Introduction

The dynamic world that we perceive around us is not 2D, but rather 3D. Unlike 2D videos, which are ubiquitous, the question of how to effectively capture, encode and disseminate free-viewpoint videos (FVV) of dynamic 3D scenes, which can be viewed at any instance of time and from any viewpoint, has intrigued computer vision and graphics researchers for much time. Free-viewpoint video transmission, if achieved, has the potential to transform and enrich user experience in profound ways by offering novel immersive experiences, *e.g.*, FVV video playback and live streaming, 3D video conferencing and telepresence, gaming, virtual spatial tutoring and teleoperation, among others.

The underlying problem of reconstructing FVV involves learning a 6D plenoptic function of a dynamic scene $P(\boldsymbol{x}, \boldsymbol{d}, t)$ from sparse multiple views acquired over a window of time, with $\boldsymbol{x} \in \mathbb{R}^3$ being a position in 3D space, $\boldsymbol{d} = (\theta, \phi)$ a viewing direction and t an instance of time. Neural volumetric representations, which learn a 5D plenoptic function of a scene $P(\boldsymbol{x}, \boldsymbol{d})$ at a fixed time instance, *e.g.*,

[*]SG's work was done during an internship at NVIDIA. [†]TL and AM contributed equally to this project. Project website: https://research.nvidia.com/labs/amri/projects/queen.

38th Conference on Neural Information Processing Systems (NeurIPS 2024).

neural radiance fields (NeRFs) [54] and its variants [2, 7, 18, 55] present a compact and high-fidelity representation for 3D scenes. NeRFs have also been extended to dynamic 4D scenes [1, 5, 19] providing a powerful tool for reconstructing FVV. However, NeRFs require compositing dense information across a 3D volume and hence are slow to train and render. Recently, 3D Gaussian Splatting (3D-GS) [29] has emerged as a promising technique with significantly faster training and rendering speeds in comparison with NeRFs, and they have also been extended to dynamic 4D scenes [42, 84, 89]. While these representations accurately model 4D scenes, they are trained in an *offline* fashion requiring full multi-view video sequences to learn temporal relationships between frames. They also require long training times to achieve high reconstruction quality and are mostly not streamable.

Online FVV, *e.g.*, for broadcast and teleconferencing applications, presents additional challenges versus offline. It requires incremental *on-the-fly* updates to volumetric representation at each time-step of the dynamic scene, *fast* training and rendering times to maintain real-time operation, and *small* packet sizes per frame to enable effective transmission on bandwidth-limited channels. Consequently, the more challenging problem of online FVV reconstruction remains relatively under-explored. Notable prior solutions are those based on NeRFs using voxel grids [37, 78] or triplanes [85] to learn 3D representations that are updated on-the-fly. Unsurprisingly, they suffer from slow rendering speeds. Recently, Sun et al. proposed 3DGStream [69], which uses 3D-GS to model a 3D scene along with InstantNGP [55] to model its geometric transformation over time. It achieves high rendering speeds but imposes heuristic structural constraints on the volumetric representation to achieve efficiency, which compromises model expressiveness and quality.

In this work, we propose a novel QUantized and Efficient ENcoding (QUEEN) framework, which uses 3D-GS for online FVV. Similarly to prior approaches [69], we also learn Gaussian attribute residuals between consecutive time-steps. To reduce memory requirements, however, [69] learns only a subset of the Gaussian attributes at each time-step, limiting model expressiveness. Our first insight, therefore, is to model residuals for *all* attributes instead, which does not compromise quality. However, encoding all Guassian attributes increases the per frame memory requirement and hence necessitates a means to compress them more effectively. Our second insight, then, is to learn to directly compress the Gaussian residuals in proportion to the real-time scene dynamics, *e.g.*, motion and illumination changes. This contrasts with existing methods [37, 69, 78, 85] that employ a single fixed-sized structure, *e.g.*, a voxel-grid, a triplane, or hash encoding at all time-steps, and the result is higher efficiency in terms of model size, training speeds, and rendering speeds. Lastly, we also exploit temporal redundancies across time-steps to limit computations to the highly dynamic parts of the scene only and achieve further efficiencies.

Specifically, to achieve this, we propose a learned quantization-sparsity framework to simultaneously learn and compress Gaussian attribute residuals for each time-step. We quantize all attribute residuals, except Gaussian positions, via an end-to-end trainable integer-based latent-decoder. Once learned, we efficiently encode the integer latents via entropy coding to achieve high compression factors. For position residuals that exhibit greater sensitivity to quantization, we propose a learned gating mechanism to sparsify them, which identifies the static (corresponding to 0 value) and dynamic Gaussians and retains the sparse dynamic ones only at full precision. Finally, to achieve further efficiencies in terms of training time and storage, we utilize the differences between the 2D viewspace Gaussian gradients of consecutive frames to initialize our learnable gates, and to selectively render local image regions corresponding to highly dynamic scene content.

We evaluate our approach, QUEEN, on two benchmark datasets, containing diverse scenes with large geometric motion and illumination changes. QUEEN outperforms all prior state-of-the-art approaches for online FVV and significantly reduces the per-frame memory cost ($\sim 10\times$), all while achieving higher reconstruction quality, as well as faster training and rendering speeds. Extensive ablations show the efficacy of the various components of our approach.

To summarize, our key contributions are:

- We propose a Gaussian residual-based framework to model 3D dynamic scenes for online FVV without any structural constraints, which allows free learning of all 3D-GS attribute residuals, resulting in higher model expressiveness.
- We introduce a learned quantization-sparsity framework for compressing per-frame residuals, and we initialize and train it efficiently using viewspace gradient differences that separate the dynamic and static scene content.

- On various challenging real-world dynamic scenes, we surpass existing state-of-the-art approaches on all metrics: reconstruction quality, memory utilization, as well as training and rendering speed.

2 Related Work

2.1 Traditional Free-viewpoint Video

Ever since early FVV work such as [27], a series of geometry-based FVV methods [12, 57] has been pushing for high reconstruction quality and streamable performance. However, their rendering and compression quality rely on the accuracy of a sophisticated pipeline of geometry reconstruction [20, 28], tracking [36], and texturing [61]. They also require high-end hardware for capturing complex and dynamic appearance [6, 14, 26]. Purely image-based rendering [10, 13, 35, 53] relaxes the requirement for geometric accuracy. Although methods such as [4, 96] support view interpolation with layered representations in the dynamic setting, they require a high count of views as input to ensure interpolation quality.

2.2 Neural and Gaussian-based Free-viewpoint Video

Offline Methods. Compared to the traditional representations, the emergence of neural representations [47, 54, 87, 67, 72] opened a new door for capturing FVV for dynamic humans [21, 31, 32, 39, 63, 83, 95] and monocular videos [22, 43, 44, 73, 75, 86]. In this work, we focus on general dynamic scenes [93] from multiple views to push the quality of streamable FVV *without* requiring a strong human prior [40, 48] or a very constrained input. [16, 62, 74, 81] model the scene dynamics via explicit deformation. Although suitable for motion analysis, they inevitably face a trade-off between motion accuracy and visual quality [74]. To tackle this, [41, 52, 59] use a spatial-temporal formulation via time-conditioned latent codes to implicitly encode the 4D scene, enabling reconstruction of topological changes and volumetric effects. [5, 19, 66] factorize the 4D scene into multiple space-time feature planes and achieves higher model compactness and training efficiency. [68, 76] decompose the 4D scene into static and dynamic volumes. [1, 46, 77, 88, 94] incorporate efficient NeRF representations [9, 19, 92] for higher fidelity. Although, these NeRF-based method achieve high compactness, they suffer from low rendering efficiency, even when converted [68] to a more efficient NeRF formulation [9, 55]. Seeing their great potential for efficiency, recent works extend 3D Gaussian representations [29] to dynamic scenes, with temporal attributes [42, 90], generalized 4D Gaussians [89] and a hybrid representation [84]. While these methods achieve high quality in modeling 3D dynamic scenes, they, together with the aforementioned NeRF-based methods, are mostly *offline*, i.e., they require all the input video and a long time for training, which is inherently difficult for streaming applications.

Online Methods. *Online* reconstruction for FVVs is relatively under-explored, as it imposes additional challenges of on-the-fly reconstruction using only local temporal information instead of the full recordings. Furthermore, toward the goal of streamable FVVs, the encoding system is evaluated by multiple metrics including compression rate, encoding and rendering speed and visual quality. [50] tracks dense 3D Gaussians by solving their motion over time. Visual quality and dynamic appearance is not their focus. [23] models motion by rendering scene dynamics, however their method is not optimized for efficiency. [45] focuses on generalizable NeRF reconstruction and shows good promise to adapt to a new frame but has a high memory footprint due to an MVSNet-style neural network [8, 91]. [37] accelerates training and rendering speed with a special tuning strategy and sparse voxels, however, their representation still has high temporal redundancy. [82] proposes an incremental training scheme with natural information partitioning and achieves high compression, but its encoding is slow. Several works [79, 80, 85] use video codec-inspired encoding paradigms for data efficiency. [79] achieves a decent compression rate and near interactive rendering with compact motion and residual grids. However, their training requires 10 minutes per frame. [80] focuses on real-time decoding, streaming and rendering instead of on-the-fly encoding. [85] performs grouped training on a hybrid representation of triplanes and volume grid. While achieving high compression rate, their fixed encoding paradigm and aggressive quantization limits their reconstruction quality along-with low rendering speeds. [69] is the closest work to ours for streaming FVV via 3D-GS. They encode the position and rotation residuals via an Instant-NGP [55] based transformation cache. While achieving faster training and rendering speeds than prior work, they have high data redundancy due to a fixed structured modeling. Additionally, they focus on geometric transformations only and

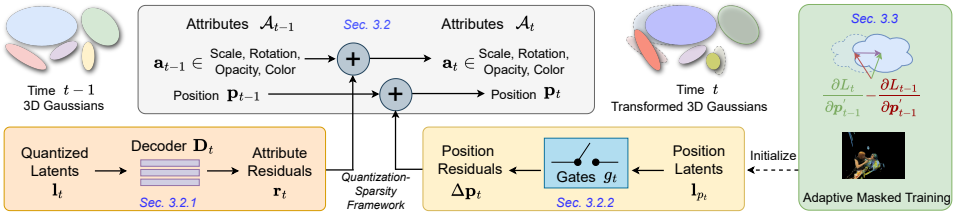

Figure 1: **Overview of QUEEN for online FVV.** We incrementally update Gaussian attributes at each time-step (gray block) by simultaneously learning and compressing residuals between consecutive time-steps via a quantization (orange block) and sparsity (yellow block) framework. We additionally render only the dynamic Gaussians for masked regions to achieve faster convergence (green block).

can approximate only small changes in new scene content or lighting variations. Our work updates and compresses all 3D-GS attributes freely without any structural constraints while still obtaining much better memory costs via our quantization-sparsity framework along with better training times.

2.3 3D Scene Representation Compression

Several works propose a variety of compression methodologies for reducing the memory, training time, or rendering speed of standard static scene 3D representations. [9, 71] decompose NeRFs via low-rank approximations. [15, 38] prune voxels along with vector quantization by [38]. [25, 70] compress multi-resolution feature-grids via codebook/vector quantization. A large number of approaches target 3D-GS compression [17, 24, 34, 58] and acceleration via pruning. While these approaches can be applied to static representations on a per-frame basis, their trivial frame-wise application would result in extremely high training costs as well as large memory per frame. To enable streaming, our work, instead, explicitly focuses on effectively leveraging the temporal redundancies across frames by compressing the residual information between them to achieve greater efficiency.

3 QUEEN: Quantized Efficient Encoding for Streaming FVV

A solution for streamable FVV must have low-latency encoding (training) and decoding (rendering), and low data bandwidth (memory) for transmission on a common network infrastructure. Motivated by these constraints, we aim to generate streamable FVVs with compact representations that are fast to train and render incrementally. In this section, we first provide an overview of 3D-GS (Sec. 3.1). In Sec. 3.2, we propose a compression framework to efficiently represent and train Gaussian attribute residuals at each time step. Sec. 3.3 discusses utilizing an approach based on viewspace gradient differences to achieve greater efficiencies. An overview of our method is shown in Fig. 1.

3.1 Preliminary: 3D Gaussian Splatting

Our efficient representation for dynamic scenes is based on 3D Gaussian Splatting (3DGS) [29]. Given multi-view images $\mathcal{I}$, a 3D scene is modeled by a set of Gaussians with attributes $\mathcal{A}$.

Representation. The shape of each Gaussian i is defined by its mean $\mathbf{p}_i \in \mathbb{R}^3$ and covariance matrix $\mathbf{\Sigma}_i$. The covariance matrix is represented by $\mathbf{\Sigma}_i = \mathbf{R}_i\mathbf{S}_i\mathbf{S}_i^T\mathbf{R}_i^T$, where $\mathbf{R}_i$ is a rotation matrix parameterized by a quaternion vector $\mathbf{q}_i \in \mathbb{R}^4$, and the scale matrix $\mathbf{S}_i$ is a diagonal matrix with elements $\mathbf{s}_i \in \mathbb{R}^3$. Each Gaussian also contains opacity $o_i \in [0, 1]$ and spherical harmonic coefficients $\mathbf{h}_i$ for view-dependent appearance with dimensions based on the number of degrees.

Rendering. For rasterization, 3D Gaussians are projected into 2D Gaussians for any given view. Given a camera with intrinsic matrix $\mathbf{K}$ and viewing transform $\mathbf{W}$, the 2D mean and covariance are:

$$\mathbf{p}'_i = \Pi(\mathbf{p}_i; \mathbf{K}, \mathbf{W}), \quad \mathbf{\Sigma}'_i = \mathbf{JW}\mathbf{\Sigma}_i\mathbf{W}^T\mathbf{J}^T, \tag{1}$$

where $\Pi(\cdot)$ denotes the perspective projection and $\mathbf{J}$ is the Jacobian of the affine approximation of the projective transform [97]. The image color $\hat{\mathbf{c}}$ at pixel location $\mathbf{x}$ is obtained by blending N depth-sorted Gaussians with their view-dependent RGB color value $\mathbf{c}_i$ computed from $\mathbf{h}_i$:

$$\hat{\mathbf{c}}(\mathbf{x}) = \sum_{i=1}^{N} \mathbf{c}_i\alpha_i \prod_{j=1}^{i-1}(1-\alpha_j), \quad \alpha_i = o_i \cdot \exp\left(-\frac{1}{2}(\mathbf{x}-\mathbf{p}'_i)^T\mathbf{\Sigma}'^{-1}_i(\mathbf{x}-\mathbf{p}'_i)\right), \tag{2}$$

where α_i is the conic opacity of Gaussian i at pixel location $\mathbf{x}$ multiplied by the Gaussian opacity o_i.

Training. With a differentiable rasterizer [29], the attributes $\mathcal{A} = \{\mathbf{p}_i, \mathbf{q}_i, \mathbf{s}_i, o_i, \mathbf{h}_i\}_{i=1}^N$ are optimized to produce renderings $\hat{\mathcal{I}} = R(\mathcal{A})$ that fit to input images $\mathcal{I}$ by optimizing a reconstruction loss which combines the D-SSIM loss [65] and L_1 loss with a hyperparameter λ:

$$L = \lambda L_{\text{D-SSIM}} + (1 - \lambda) L_1. \tag{3}$$

3.2 Attribute Residual Compression

Given a multi-view image sequence $\{\mathcal{I}_t\}_{t=0}^{T-1}$, our goal is to reconstruct the dynamic scene via Gaussian attributes $\mathcal{A}_t$ for each time-step t. We model the attributes based on the trained attributes from the previous time-step $t-1$ as

$$\mathcal{A}_t = \mathcal{A}_{t-1} + \mathcal{R}_t, \tag{4}$$

where $\mathcal{R}_t$ consists of learnable residuals for each attribute (in Fig. 1 (gray block)). For time-step $t = 0$, we perform vanilla Gaussian splatting training to obtain attributes $\mathcal{A}_0$. This sequential formulation allows us to freely and adaptively update the residuals $\mathcal{R}_t$ on-the-fly with incoming streaming training views, without any structural constraints as in prior works [69]. However, representing the 4D scene with uncompressed residuals is still highly inefficient. As residuals have low magnitudes in comparison with the attributes themselves, they can be efficiently compressed, for which we propose a novel quantization-sparsity framework.

3.2.1 Attribute Residual Quantization

There exists spatial redundancy within the Gaussian attributes of the same time-step. Nearby Gaussians have highly correlated residuals for shape, orientation and appearance. To reduce the storage cost of the residuals, we propose to utilize a quantization framework during training [24].

At each time-step t, we represent the residuals via quantized latents and a shared compact decoder. Specifically, to obtain the residuals for each category[2] $\mathbf{r}_i \in \mathbb{R}^M$, we maintain corresponding quantized integer latents $\mathbf{l}_i \in \mathbb{Z}^L$ for each Gaussian i. These latents are passed through a shared linear decoder D with learnable parameters $\mathbf{D} \in \mathbb{R}^{M \times L}$ to obtain the decoded attribute residual $\mathbf{r}_i$. Such a compact decoder has small time and memory costs due to few parameters and arithmetic operations. To allow differentiable training of the integer latents via gradient optimization, we use a continuous approximation $\hat{\mathbf{l}}_i \in \mathbb{R}^L$ instead. $\hat{\mathbf{l}}_i$ are rounded to the nearest integer values for the forward pass but can still receive backpropagated gradients via the Straight-Through Estimator (STE) [3]:

$$\mathbf{l}_i = \text{STE}(\hat{\mathbf{l}}_i), \quad \mathbf{r}_i = D(\mathbf{l}_i; \mathbf{D}) = \mathbf{D} \cdot \text{float}(\mathbf{l}_i). \tag{5}$$

The continuous latents $\hat{\mathbf{L}} = \{\hat{\mathbf{l}}_i\}_{i=1}^N$, and the shared decoder's parameters $\mathbf{D}$ are learnable during training. After adding the decoded residuals to the previous time-step's attributes (Eq. 4), the standard rasterization process (Eq. 2) is used to obtain the rendered image. This differentiable quantization module is trained end-to-end with the main training process by optimizing the reconstruction loss. Post-training, we entropy code the quantized latents $\mathbf{L}$ and directly store the decoder $\mathbf{D}$. Entropy coding results in as much as $10\times$ reduction in model size from 44 to 4 MB without quality degradation.

3.2.2 Position Residual Gating

Sparse Representation. While most of the attribute residuals can be quantized effectively with our proposed method in Sec 3.2.1, we observe that the position residuals are sensitive to quantization and require high precision during rendering[3]. Storing all the full-precision position residuals, however, still results in high per-frame memory costs. To tackle this, we propose a learned gating methodology, which enforces sparsity in the residuals instead of quantization. This mechanism allows us to set a vast majority of the position residuals to zeros, while maintaining full-precision non-zero values. Specifically, we represent the positional residual for each Gaussian i as $\Delta\mathbf{p}_i = g_i \cdot \mathbf{l}_{p_i}$, where the scalar g_i is the learnable gate variable and $\mathbf{l}_{p_i} \in \mathbb{R}^3$ is the learnable pre-gated residual in full precision during training. After training, the sparse $\Delta\mathbf{p}_i$ can be efficiently stored via sparse matrix formats [60] to reduce memory costs. Thus, our goal is to encourage the sparsity for the variable g_i across all

[2] $\mathbf{r} \in \mathcal{R}$, belong to one of five categories of Gaussian attributes: position, rotation, scale, opacity and color.

[3] Concurrent work [58] also discovered that positional attributes are sensitive to compression.

Gaussians. This goal also aligns with the observation that a large portion of a dynamic scene is static or nearly static, which can be leveraged to attain high compression performance.

Hard Concrete Gate. Sparsity can be induced via L_0 or L_1 norm regularization penalties. However, L_1 norm induces shrinkage, *i.e.*, lowers the magnitude of even non-zero values. L_0 norm is the ideal sparsity loss without shrinkage, but is computationally intractable with non-differentiability and combinatorial complexity. To enforce sparsity, we instead propose to use the hard concrete gate [49]. For each Gaussian i, the concrete gate [51] is a continuous relaxation of the Bernoulli distribution:

$$\hat{g}_i = \text{Sigmoid}(\log \alpha_i / \tau), \tag{6}$$

where α_i is a learnable parameter and τ is the temperature parameter. Although the concrete gate approximates the discrete Bernoulli gate, it does not include the end points $\{0, 1\}$, which does not directly result in sparsity. The hard concrete gate "stretches" the range of the concrete gate to the interval (γ_0, γ_1) and then applies a hard-sigmoid:

$$\widetilde{g}_i = \hat{g}_i \cdot (\gamma_1 - \gamma_0) + \gamma_0, \quad g_i = \min(1, \max(0, \widetilde{g}_i)). \tag{7}$$

This includes the end points $\{0, 1\}$ for g_i, required for achieving sparse residuals.

Sparsity Loss. The hard concrete gate formulation leads to a convenient regularization loss for encouraging L_0 sparsity [49] in the gates g_i:

$$L_{\text{reg}} = \sum_{i=1}^{N} p_i = \sum_{i=1}^{N} \text{Sigmoid}\left(\log \alpha_i - \tau \log \frac{-\gamma_0}{\gamma_1}\right). \tag{8}$$

Here, we treat $\boldsymbol{\alpha} = \{\alpha_i\}_{i=1}^{N}$ to be learnable parameters for all N Gaussians at a given time-step and $\{\tau, \gamma_0, \gamma_1\}$ as hyperparameters that are shared for all Gaussians and all time-steps.

3.3 Viewspace Gradient Difference for Adaptive Training

Real-world dynamic scenes contain high amounts of temporal redundancy with only a fraction of the content changing between consecutive time-steps. The proposed quantization-sparsity framework can learn to identify Gaussians corresponding to static scene content and set their residuals to 0. However, they still forward/backward pass through static regions resulting in wasted training computation. Additionally, initializing the gates with 1s requires more iterations for convergence. We thus propose a proxy metric to identify Gaussians, which are static or dynamic at the start of training. We use this metric to initialize our gates while also identifying dynamic image regions to perform local rendering in, during training.

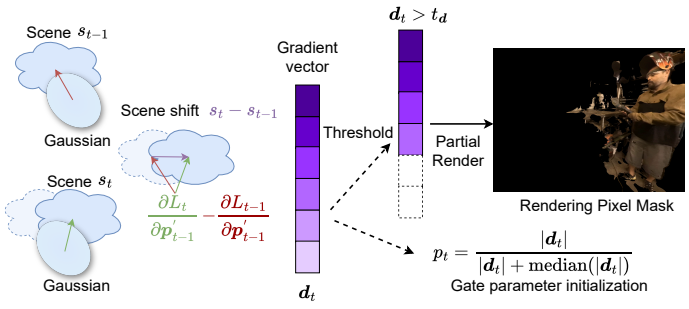

Figure 2: **Viewspace Gradient Difference.** We use the difference of viewspace gradients between consecutive frames to identify dynamic scene content.

Viewspace Gradient Difference. The ground-truth (GT) training images contain information of the dynamic scene content, which we leverage to separate static and dynamic Gaussians. A simple pixel difference between consecutive frames does not account for illumination changes and is a noisy signal for the geometric position residuals. 3D-GS utilizes 2D viewspace gradients $\frac{\partial L}{\partial \mathbf{p}'}$ to identify poorly fitted Gaussians based on the reconstruction loss L between the rendered ($\hat{\mathcal{I}}$), GT image ($\mathcal{I}$).

More concretely, after training Gaussians at time-step $t-1$ with an MSE loss, L_{t-1} and 2D Gaussian means $\mathbf{p}'_{t-1}$, we compute the MSE loss for the next time-step L_t and then compute the gradient difference. The score vector $\mathbf{d}_t$ is the average of gradient differences across all training views v:

$$\mathbf{d}_t = \frac{1}{V} \sum_{v=0}^{V-1} \left[\frac{\partial L_t^{(v)}}{\partial \boldsymbol{p'}_{t-1}^{(v)}} - \frac{\partial L_{t-1}^{(v)}}{\partial \boldsymbol{p'}_{t-1}^{(v)}} \right], \quad L_{t-1}^{(v)} = L\left(\mathcal{I}_{t-1}^{(v)}, \hat{\mathcal{I}}_{t-1}^{(v)}\right), \quad L_t^{(v)} = L\left(\mathcal{I}_t^{(v)}, \hat{\mathcal{I}}_{t-1}^{(v)}\right). \tag{9}$$

As shown in Fig. 2, $\boldsymbol{d}_t$ identifies the dynamic scene regions while factoring out the noise from imperfect reconstructions at time-step $t-1$. We use the norm of the score vector $|\mathbf{d}_{t_i}|$ to initialize the gate parameters. We define the probability of a gate being active for Gaussian i at time-step t as

$$d_{t_i} = \frac{|\mathbf{d}_{t_i}|}{|\mathbf{d}_{t_i}| + \underset{i=1,2,\ldots,N}{\text{median}}(|\mathbf{d}_{t_i}|)}. \tag{10}$$

We set p_i in Eq. 8 to be d_{t_i} to solve for the initial α_i. This initialization leads to better convergence by identifying Gaussians corresponding to 0 position residuals at the start of training itself.

Adaptive Masked Training. In addition to gate initialization, we propose to utilize the score vector $\boldsymbol{d}_t$ for an adaptive masked training scheme. We split the Gaussians into static or dynamic parts by applying a threshold $t_{\mathbf{d}}$ on the norm of $\boldsymbol{d}_t$. We render dynamic Gaussians for each training view to identify corresponding dynamic image regions. We then only render and backpropagate through these pixel locations. We perform this masked training for a fraction of the full training iterations, and find it to improve training speeds with little to no loss of reconstruction quality.

3.4 Efficient End-to-end Learnable Residuals

Initial Frame Reconstruction. For an incrementally updating online approach, it is important to make sure the initial frame is well reconstructed. COLMAP used to initialize the positions of Gaussians can result in sparse 3D points for regions with sparse camera views. Hence, we use an off-the-shelf monocular depth estimation network to estimate point locations in these empty regions and predict a more complete initial point cloud. Further details and results are in the supplementary.

End-to-end Training. We train separate decoders and quantized latents $\{\mathbf{L}_c, \mathbf{D}_c | c \in \{\boldsymbol{q}, \boldsymbol{s}, o, \boldsymbol{h}\}\}$ for all attributes except position. For position, we learn the gate parameters $\boldsymbol{\alpha}$ and positional residuals $\mathbf{L}_p$. All variables are end-to-end differentiable. The total loss function that we minimize is the reconstruction loss (Eq. 3) and the sparsity gate regularization loss (Eq. 8):

$$L_{\text{total}} = L + \lambda_{\text{reg}} L_{\text{reg}}, \tag{11}$$

where λ_{reg} controls tradeoffs between memory and reconstruction quality. By simultaneously quantizing while training we achieve high compression while maintaining quality, unlike [85, 79] with post-training compression that lead to quality degradations. We also apply the 3D-GS densification stage at each time-step and is sufficient in modeling new or finer scene content. 3DGStream [69] adds Gaussians relative to the first time-step only, which limits their approach to small scene changes.

4 Experiments

4.1 Datasets and Implementation

We evaluate our method on two challenging FVV video datasets. **(1) Neural 3D Videos (N3DV)** [41] consists of six indoor scenes with forward-facing 20-view videos. **(2) Immersive Videos** [4] consists of seven indoor and outdoor scenes captures with 46 cameras. In both datasets, the central view is held out for testing. We implement QUEEN on [29]. We train for 500 and 350 epochs for the first time-step, and for 10 and 15 epochs for the subsequent time-steps, for N3DV and Immersive, respectively, on an NVIDIA A100 GPU. One epoch contains all training views. We evaluate visual quality in terms of average frame-wise PSNR, SSIM, and LPIPS (VGG) across all videos. We also compute the average storage size and training time for each time-step, and the rendering speed. Additional details are provided in the supplementary materials.

4.2 Quantitative Comparisons

We compare QUEEN against state-of-the-art existing online FVV methods (3DGStream [69], StreamRF [37] and TeTriRF [85]) on N3DV and Immersive (Tab. 1). 3DGStream [69] is the overall best-performing prior method. Since 3DGStream [69] was originally run on an older NVIDIA V100 GPU on N3DV, we re-run 3DGStream on an NVIDIA A100 GPU on both N3DV and Immersive and denote it as 3DGStream* in Tab. 1 for consistency with QUEEN. For brevity, in Tab. 1 we additionally compare against only selected top-performing offline FVV methods. We include a more extensive comparison to all existing offline FVV methods in the supplementary (Tab. 8). Lastly, we evaluate three variants of QUEEN: QUEEN-s (small), QUEEN-m (medium) and QUEEN-l (large), with residuals trained for 6, 8 and 10 epochs, respectively.

Table 1: **Quantitative Results.** We compare QUEEN against state-of-the-art online and (a few for brevity) offline FVV methods on N3DV [41] and Immersive [4]. We include many more offline methods in the supplementary (Tab. 8). 3DGStream* refers to our re-implementation on the same NVIDIA A100 GPU used by QUEEN for fairness. Bold and underlined numbers indicate the **best** and the second best results, respectively, within each category.

Neural 3D Video (N3DV) dataset

Category	Method	PSNR (dB) ↑	SSIM ↑	LPIPS ↓	Storage (MB) ↓	Training (sec) ↓	Rendering (FPS) ↑
Offline	NeRFPlayer [68]	30.69	0.932	0.209	17.10	72	0.05
	HyperReel [1]	31.10	0.928	-	1.20	104	2.00
	SpaceTime [42]	**32.05**	**0.948**	-	**0.67**	**20**	**140**
Online	StreamRF [37]	30.68	-	-	31.4	15	8.3
	TeTriRF [85]	30.43	0.906	0.248	**0.06**	39	4
	3DGStream [69]	31.67	-	-	7.83	12	215
	3DGStream* [69]	31.58	0.941	0.140	7.80	8.5	261
	QUEEN-s (ours)	31.89	0.945	0.139	0.68	**4.65**	**345**
	QUEEN-m (ours)	32.03	0.946	0.137	0.69	5.96	321
	QUEEN-l (ours)	**32.19**	**0.946**	**0.136**	0.75	7.9	248

Immersive dataset

Category	Method	PSNR (dB) ↑	SSIM ↑	LPIPS ↓	Storage (MB) ↓	Training (sec) ↓	Rendering (FPS) ↑
Offline	NeRFPlayer [68]	25.8	0.848	0.329	17.1	∼72	0.12
	HyperReel [1]	28.8	0.874	-	1.2	∼108	4
	SpaceTime [42]	**29.2**	**0.916**	-	**1.2**	∼**72**	**99**
Online	3DGStream* [69]	25.18	0.876	0.255	8.83	32.4	**221**
	QUEEN-l (ours)	**29.22**	**0.915**	**0.208**	**1.79**	**19.7**	183

Table 2: **Effect of Various Components Ablated on N3DV and Immersive Datasets.**

Components	N3DV				Immersive			
	PSNR (dB) ↑	Storage (MB) ↓	Training (sec) ↓	Rendering (FPS) ↑	PSNR (dB) ↑	Storage (MB) ↓	Training (sec) ↓	Rendering (FPS) ↑
Baseline	31.66	44.36	7.29	214	28.54	78.4	20.85	**276**
+ Attribute Quantization	32.04	4.18	**7.28**	**285**	29.01	4.57	25.17	199
+ Position Gating	32.05	0.72	6.95	274	28.99	**2.01**	26.99	190
+ Gate Initialization	32.14	**0.60**	7.92	271	29.08	**1.33**	27.81	177
+ Masked Training	**32.19**	0.74	7.88	248	**29.22**	1.79	**19.70**	183

From Tab. 1, on N3DV, QUEEN-l results in the best quality among all online FVV methods and achieves a $10\times$ reduction in storage size compared to 3DGStream. Although TeTriRF requires less memory than QUEEN, it has much worse quality (-1.5dB) and rendering speed (4FPS), and higher training time (39 sec). On Immersive, which contains more pronounced scene changes than N3DV, we limit our comparisons to 3DGStream with longer iterations. TeTriRF requires long convergence times to achieve reasonable reconstruction quality, limiting their training feasibility. QUEEN-l significantly outperforms 3DGStream, obtaining $+4$dB PSNR, $5\times$ smaller size, and lower training times. These results on the more challenging scenes from the Immersive datasets reveal the structural constraints brought by the heuristic compression design of 3DGStream. In contrast, our quantization-sparsity framework shows higher flexibility and quality in capturing changing appearances and scene density as well as learning compact and effective representations.

4.3 Qualitative Comparisons

In Fig. 3 we compare the reconstruction results of the various methods. On N3DV, we reconstruct finer details than 3DGStream, *e.g.*, the hand and the dog, and minimize artifacts such as the tongs in the top scene or the coffee and metal tumbler in the bottom scene. TeTriRF produces blurry outputs, *e.g.*, the cap or metal tumbler in the bottom scene. On Immersive, we better model illumination changes and new scene content such as the person (first patch) and the flame (third patch) in the top scene or the face in the bottom scene (second patch) versus 3DGStream.

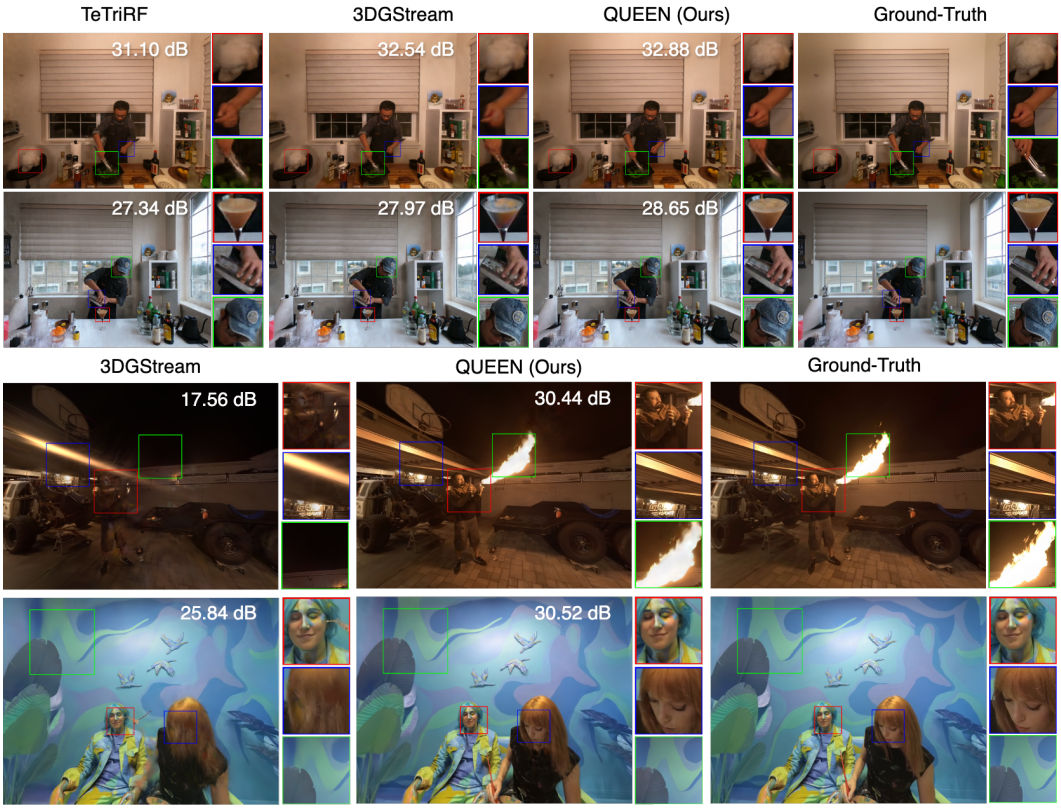

Figure 3: **Qualitative Results.** A visualization of various scenes in the N3DV and Immersive datasets. PSNR (↑) values are shown. We include additional video results in the supplement.

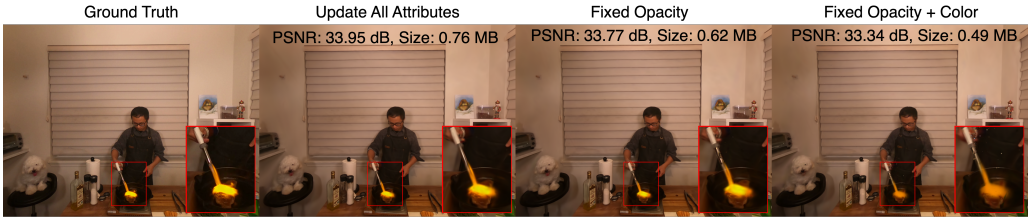

Figure 4: **Effect of Updating Appearance Attributes.** QUEEN updates all Gaussian attributes, resulting in improved quality versus keeping appearance attributes fixed across a video.

4.4 Ablations

Effect of Updating Appearance Attributes. To ablate the importance of updating the Gaussian appearance attributes (color and opacity) per frame in QUEEN, we run experiments on N3DV for 2 settings: (1) learning only geometric attribute residuals (position, scale and covariance) with appearance residuals set to zero and (2) learning all residuals per frame (Tab. 3). Updating only geometric attributes results in a drop of 0.4 dB PSNR versus updating all attributes.Visually, for the Flame Steak scene in N3DV (Fig. 4), updating all attributes results in the highest quality, while fixing opacity introduces artifacts at the edge of the flamethrower. Fixing color, additionally, results in a significant drop in PSNR (-0.6 dB) producing a discolored flame (rightmost column).

Effect of Attribute Compression and Masked Training. We show results for five variants of QUEEN with incrementally added sub-components: (1) a baseline with uncompressed residual training (Sec. 3.2), (2) adding quantization to all attributes except position (Sec. 3.2.1), (3) adding gating of position residuals (Sec. 3.2.2), (4) gate initialization with viewspace gradient differences and (5) masked image training (Sec. 3.3). Results are summarized in Tab. 2 for both N3DV and Immersive datasets. Compressing attributes and gating position residuals results in significant model size reduction on both datasets ($60\times, 40\times$). This is further reduced by gate initialization with

Table 3: **Updating Appearance Attributes on N3DV.** PSNR significantly improves by updating all attributes but with a small storage overhead.

Update Attributes	PSNR (dB)	Storage (MB)	Train. (sec)
Geometric	31.61	**0.61**	7.87
+ Appearance	**32.03**	0.74	**7.57**

Table 4: **Effect of Quantizing Scaling Attribute on N3DV.** PSNR improves while also reducing model size and training time due to faster rendering.

Configuration	PSNR (dB)	Storage (MB)	Train. (sec)
w/o Scaling Quant.	31.69	4.39	11.01
w/ Scaling Quant.	**32.08**	**0.69**	**7.07**

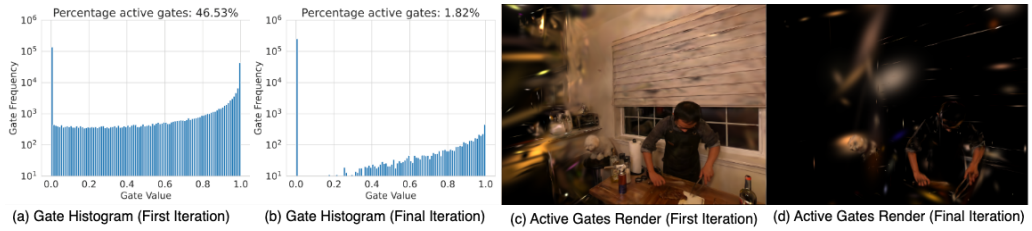

(a) Gate Histogram (First Iteration) (b) Gate Histogram (Final Iteration) (c) Active Gates Render (First Iteration) (d) Active Gates Render (Final Iteration)

Figure 5: **Effect of Gating.** While a large number of gates (47%) are active at start of training (a, c), they are pruned and only gates corresponding to changing scene content (2%) remain active (b, d).

viewspace gradient differences due to faster convergence of the gates, without loss of quality. By masked training via localized image rendering, we reduce training time by 8 seconds for Immersive and marginally for N3DV. Overall, from the baseline, we obtain significant model size reduction with equivalent or lower training and rendering speed. Attribute quantization framework even improves PSNR compared to the baseline for both datasets. This largely stems from quantizing the scaling attribute leading to a more stable optimization with better reconstruction quality while reducing storage size (Tab. 4).

Effect of Gating. As shown in Fig. 5, more than half of the gates are set to be inactive at the start of training with viewspace gradient initialization (Sec. 3.3) and a large portion of the image is active. However, post-training, most gates become inactive while the remaining active gates successfully focus on the dynamic scene content, *e.g.*, the person's hands or the dog's face. This validates that our gating mechanism effectively separates static and dynamic scene content.

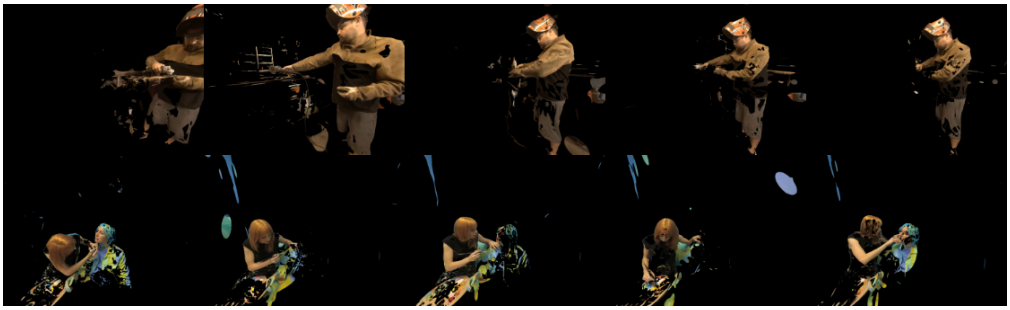

Figure 6: **Adaptive Image Mask Visualization.** We separate out the dynamic scene content at different time-steps of the video through our viewspace gradient difference approach in Sec. 3.3.

Effect of Adaptive Image Mask. We visualize the masks obtained by our viewspace gradient difference module in Sec. 3.3. Results on 2 scenes in the Immersive dataset are shown in Fig. 6. For various time instance of the video (columns), we adaptively identify image regions corresponding to the dynamic scene content. We can therefore perform local image rendering and backpropagation for faster training skipping computation for the static parts of the scene such as the background.

5 Conclusion

We proposed QUEEN, a framework to model 3D dynamic scenes for online FVV using 3D-GS. We utilized an attribute residual framework, which freely updates all parameters leading to better modeling of complex scenes. We show that the residuals can be successfully compressed via our learned quantization-sparsity mechanism, which adapts to the dynamic scene content to achieve very small model sizes, improved training and rendering speeds, and improved visual quality. In future work, we aim to extend QUEEN for sparse view reconstruction or sequences with long duration.

References

[1] Benjamin Attal, Jia-Bin Huang, Christian Richardt, Michael Zollhoefer, Johannes Kopf, Matthew O'Toole, and Changil Kim. Hyperreel: High-fidelity 6-dof video with ray-conditioned sampling. In *Proceedings of the IEEE/CVF Conference on Computer Vision and Pattern Recognition*, pages 16610–16620, 2023.

[2] Jonathan T Barron, Ben Mildenhall, Matthew Tancik, Peter Hedman, Ricardo Martin-Brualla, and Pratul P Srinivasan. Mip-nerf: A multiscale representation for anti-aliasing neural radiance fields. In *Proceedings of the IEEE/CVF International Conference on Computer Vision*, pages 5855–5864, 2021.

[3] Yoshua Bengio, Nicholas Léonard, and Aaron Courville. Estimating or propagating gradients through stochastic neurons for conditional computation. *arXiv preprint arXiv:1308.3432*, 2013.

[4] Michael Broxton, John Flynn, Ryan Overbeck, Daniel Erickson, Peter Hedman, Matthew Duvall, Jason Dourgarian, Jay Busch, Matt Whalen, and Paul Debevec. Immersive light field video with a layered mesh representation. *ACM Transactions on Graphics (TOG)*, 39(4):86–1, 2020.

[5] Ang Cao and Justin Johnson. Hexplane: A fast representation for dynamic scenes. In *Proceedings of the IEEE/CVF Conference on Computer Vision and Pattern Recognition*, pages 130–141, 2023.

[6] Charles-Félix Chabert, Per Einarsson, Andrew Jones, Bruce Lamond, Wan-Chun Ma, Sebastian Sylwan, Tim Hawkins, and Paul Debevec. Relighting human locomotion with flowed reflectance fields. In *ACM SIGGRAPH 2006 Sketches*, pages 76–es. Association for Computing Machinery, 2006.

[7] Eric R Chan, Connor Z Lin, Matthew A Chan, Koki Nagano, Boxiao Pan, Shalini De Mello, Orazio Gallo, Leonidas J Guibas, Jonathan Tremblay, Sameh Khamis, et al. Efficient geometry-aware 3d generative adversarial networks. In *Proceedings of the IEEE/CVF conference on computer vision and pattern recognition*, pages 16123–16133, 2022.

[8] Anpei Chen, Zexiang Xu, Fuqiang Zhao, Xiaoshuai Zhang, Fanbo Xiang, Jingyi Yu, and Hao Su. Mvsnerf: Fast generalizable radiance field reconstruction from multi-view stereo. In *Proceedings of the IEEE/CVF international conference on computer vision*, pages 14124–14133, 2021.

[9] Anpei Chen, Zexiang Xu, Andreas Geiger, Jingyi Yu, and Hao Su. Tensorf: Tensorial radiance fields. In *European Conference on Computer Vision*, pages 333–350. Springer, 2022.

[10] Shenchang Eric Chen and Lance Williams. View interpolation for image synthesis. In *Proceedings of the 20th annual conference on Computer graphics and interactive techniques*, pages 279–288, 1993.

[11] Hye Won Chung, Brian M Sadler, and Alfred O Hero. Bounds on variance for unimodal distributions. *IEEE Transactions on Information Theory*, 63(11):6936–6949, 2017.

[12] Alvaro Collet, Ming Chuang, Pat Sweeney, Don Gillett, Dennis Evseev, David Calabrese, Hugues Hoppe, Adam Kirk, and Steve Sullivan. High-quality streamable free-viewpoint video. *ACM Transactions on Graphics (ToG)*, 34(4):1–13, 2015.

[13] Abe Davis, Marc Levoy, and Fredo Durand. Unstructured light fields. *Comput. Graph. Forum*, 31(2pt1):305–314, may 2012. ISSN 0167-7055. doi: 10.1111/j.1467-8659.2012.03009.x. URL `https://doi.org/10.1111/j.1467-8659.2012.03009.x`.

[14] Paul Debevec, Tim Hawkins, Chris Tchou, Haarm-Pieter Duiker, Westley Sarokin, and Mark Sagar. Acquiring the reflectance field of a human face. In *Proceedings of the 27th annual conference on Computer graphics and interactive techniques*, pages 145–156, 2000.

[15] Chenxi Lola Deng and Enzo Tartaglione. Compressing explicit voxel grid representations: fast nerfs become also small. In *Proceedings of the IEEE/CVF Winter Conference on Applications of Computer Vision*, pages 1236–1245, 2023.

[16] Yilun Du, Yinan Zhang, Hong-Xing Yu, Joshua B Tenenbaum, and Jiajun Wu. Neural radiance flow for 4d view synthesis and video processing. In *2021 IEEE/CVF International Conference on Computer Vision (ICCV)*, pages 14304–14314. IEEE Computer Society, 2021.

[17] Zhiwen Fan, Kevin Wang, Kairun Wen, Zehao Zhu, Dejia Xu, and Zhangyang Wang. Lightgaussian: Unbounded 3d gaussian compression with 15x reduction and 200+ fps. *arXiv preprint arXiv:2311.17245*, 2023.

[18] Sara Fridovich-Keil, Alex Yu, Matthew Tancik, Qinhong Chen, Benjamin Recht, and Angjoo Kanazawa. Plenoxels: Radiance fields without neural networks. In *Proceedings of the IEEE/CVF Conference on Computer Vision and Pattern Recognition*, pages 5501–5510, 2022.

[19] Sara Fridovich-Keil, Giacomo Meanti, Frederik Rahbæk Warburg, Benjamin Recht, and Angjoo Kanazawa. K-planes: Explicit radiance fields in space, time, and appearance. In *Proceedings of the IEEE/CVF Conference on Computer Vision and Pattern Recognition*, pages 12479–12488, 2023.

[20] Jean Furukawa, Yasutaka; Ponce. Accurate, dense, and robust multiview stereopsis. *IEEE TRANSACTIONS ON PATTERN ANALYSIS AND MACHINE INTELLIGENCE*, 32(8), 2010.

[21] Guy Gafni, Justus Thies, Michael Zollhofer, and Matthias Nießner. Dynamic neural radiance fields for monocular 4d facial avatar reconstruction. In *Proceedings of the IEEE/CVF Conference on Computer Vision and Pattern Recognition*, pages 8649–8658, 2021.

[22] Chen Gao, Ayush Saraf, Johannes Kopf, and Jia-Bin Huang. Dynamic view synthesis from dynamic monocular video. In *Proceedings of the IEEE International Conference on Computer Vision*, 2021.

[23] Quankai Gao, Qiangeng Xu, Zhe Cao, Ben Mildenhall, Wenchao Ma, Le Chen, Danhang Tang, and Ulrich Neumann. Gaussianflow: Splatting gaussian dynamics for 4d content creation. *arXiv preprint arXiv:2403.12365*, 2024.

[24] Sharath Girish, Kamal Gupta, and Abhinav Shrivastava. Eagles: Efficient accelerated 3d gaussians with lightweight encodings. *arXiv preprint arXiv:2312.04564*, 2023.

[25] Sharath Girish, Abhinav Shrivastava, and Kamal Gupta. Shacira: Scalable hash-grid compression for implicit neural representations. In *Proceedings of the IEEE/CVF International Conference on Computer Vision (ICCV)*, pages 17513–17524, October 2023.

[26] Kaiwen Guo, Peter Lincoln, Philip Davidson, Jay Busch, Xueming Yu, Matt Whalen, Geoff Harvey, Sergio Orts-Escolano, Rohit Pandey, Jason Dourgarian, et al. The relightables: Volumetric performance capture of humans with realistic relighting. *ACM Transactions on Graphics (ToG)*, 38(6):1–19, 2019.

[27] Takeo Kanade, Peter Rander, and PJ Narayanan. Virtualized reality: Constructing virtual worlds from real scenes. *IEEE Multimedia*, 4(1):34–47, 1997.

[28] Michael Kazhdan and Hugues Hoppe. Screened poisson surface reconstruction. *ACM Transactions on Graphics (ToG)*, 32(3):1–13, 2013.

[29] Bernhard Kerbl, Georgios Kopanas, Thomas Leimkühler, and George Drettakis. 3d gaussian splatting for real-time radiance field rendering. *ACM Transactions on Graphics*, 42(4):1–14, 2023.

[30] Diederik P Kingma and Jimmy Ba. Adam: A method for stochastic optimization. *arXiv preprint arXiv:1412.6980*, 2014.

[31] Tobias Kirschstein, Shenhan Qian, Simon Giebenhain, Tim Walter, and Matthias Nießner. Nersemble: Multi-view radiance field reconstruction of human heads. *ACM Trans. Graph.*, 42(4), jul 2023. ISSN 0730-0301. doi: 10.1145/3592455. URL https://doi.org/10.1145/3592455.

[32] Muhammed Kocabas, Rick Chang, James Gabriel, Oncel Tuzel, and Anurag Ranjan. Hugs: Human gaussian splats, 2023. URL https://arxiv.org/abs/2311.17910.

[33] Glen G Langdon. An introduction to arithmetic coding. *IBM Journal of Research and Development*, 28(2):135–149, 1984.

[34] Joo Chan Lee, Daniel Rho, Xiangyu Sun, Jong Hwan Ko, and Eunbyung Park. Compact 3d gaussian representation for radiance field. *arXiv preprint arXiv:2311.13681*, 2023.

[35] Marc Levoy and Pat Hanrahan. Light field rendering. In *Proceedings of the 23rd annual conference on Computer graphics and interactive techniques*, pages 31–42, 1996.

[36] Hao Li, Bart Adams, Leonidas J. Guibas, and Mark Pauly. Robust single-view geometry and motion reconstruction. *ACM Transactions on Graphics (Proceedings SIGGRAPH Asia 2009)*, 28(5), December 2009.

[37] Lingzhi Li, Zhen Shen, Zhongshu Wang, Li Shen, and Ping Tan. Streaming radiance fields for 3d video synthesis. *Advances in Neural Information Processing Systems*, 35:13485–13498, 2022.

[38] Lingzhi Li, Zhen Shen, Zhongshu Wang, Li Shen, and Liefeng Bo. Compressing volumetric radiance fields to 1 mb. In *Proceedings of the IEEE/CVF Conference on Computer Vision and Pattern Recognition*, pages 4222–4231, 2023.

[39] Ruilong Li, Julian Tanke, Minh Vo, Michael Zollhöfer, Jürgen Gall, Angjoo Kanazawa, and Christoph Lassner. Tava: Template-free animatable volumetric actors. In *European Conference on Computer Vision*, pages 419–436. Springer, 2022.

[40] Tianye Li, Timo Bolkart, Michael. J. Black, Hao Li, and Javier Romero. Learning a model of facial shape and expression from 4D scans. *ACM Transactions on Graphics, (Proc. SIGGRAPH Asia)*, 36(6):194:1–194:17, 2017. URL `https://doi.org/10.1145/3130800.3130813`.

[41] Tianye Li, Mira Slavcheva, Michael Zollhoefer, Simon Green, Christoph Lassner, Changil Kim, Tanner Schmidt, Steven Lovegrove, Michael Goesele, Richard Newcombe, et al. Neural 3d video synthesis from multi-view video. In *Proceedings of the IEEE/CVF Conference on Computer Vision and Pattern Recognition*, pages 5521–5531, 2022.

[42] Zhan Li, Zhang Chen, Zhong Li, and Yi Xu. Spacetime gaussian feature splatting for real-time dynamic view synthesis. In *Proceedings of the IEEE/CVF Conference on Computer Vision and Pattern Recognition*, 2024.

[43] Zhengqi Li, Simon Niklaus, Noah Snavely, and Oliver Wang. Neural scene flow fields for space-time view synthesis of dynamic scenes. In *Proceedings of the IEEE/CVF Conference on Computer Vision and Pattern Recognition*, pages 6498–6508, 2021.

[44] Zhengqi Li, Qianqian Wang, Forrester Cole, Richard Tucker, and Noah Snavely. Dynibar: Neural dynamic image-based rendering. In *Proceedings of the IEEE/CVF Conference on Computer Vision and Pattern Recognition (CVPR)*, 2023.

[45] Haotong Lin, Sida Peng, Zhen Xu, Yunzhi Yan, Qing Shuai, Hujun Bao, and Xiaowei Zhou. Efficient neural radiance fields for interactive free-viewpoint video. In *SIGGRAPH Asia 2022 Conference Papers*, pages 1–9, 2022.

[46] Haotong Lin, Sida Peng, Zhen Xu, Tao Xie, Xingyi He, Hujun Bao, and Xiaowei Zhou. High-fidelity and real-time novel view synthesis for dynamic scenes. In *SIGGRAPH Asia 2023 Conference Papers*, pages 1–9, 2023.

[47] Stephen Lombardi, Tomas Simon, Jason Saragih, Gabriel Schwartz, Andreas Lehrmann, and Yaser Sheikh. Neural volumes: Learning dynamic renderable volumes from images. *ACM Transactions on Graphics*, 38(4):65:1–65:14, July 2019.

[48] Matthew Loper, Naureen Mahmood, Javier Romero, Gerard Pons-Moll, and Michael J. Black. SMPL: A skinned multi-person linear model. *ACM Trans. Graphics (Proc. SIGGRAPH Asia)*, 34(6):248:1–248:16, October 2015.

[49] Christos Louizos, Max Welling, and Diederik P Kingma. Learning sparse neural networks through L_0 regularization. *arXiv preprint arXiv:1712.01312*, 2017.

[50] Jonathon Luiten, Georgios Kopanas, Bastian Leibe, and Deva Ramanan. Dynamic 3d gaussians: Tracking by persistent dynamic view synthesis. In *3DV*, 2024.

[51] Chris J Maddison, Andriy Mnih, and Yee Whye Teh. The concrete distribution: A continuous relaxation of discrete random variables. *arXiv preprint arXiv:1611.00712*, 2016.

[52] Ricardo Martin-Brualla, Noha Radwan, Mehdi SM Sajjadi, Jonathan T Barron, Alexey Dosovitskiy, and Daniel Duckworth. Nerf in the wild: Neural radiance fields for unconstrained photo collections. In *Proceedings of the IEEE/CVF Conference on Computer Vision and Pattern Recognition*, pages 7210–7219, 2021.

[53] Ben Mildenhall, Pratul P Srinivasan, Rodrigo Ortiz-Cayon, Nima Khademi Kalantari, Ravi Ramamoorthi, Ren Ng, and Abhishek Kar. Local light field fusion: Practical view synthesis with prescriptive sampling guidelines. *ACM Transactions on Graphics (TOG)*, 38(4):1–14, 2019.

[54] Ben Mildenhall, Pratul P Srinivasan, Matthew Tancik, Jonathan T Barron, Ravi Ramamoorthi, and Ren Ng. NeRF: Representing scenes as neural radiance fields for view synthesis. In *European Conference on Computer Vision*, 2020.

[55] Thomas Müller, Alex Evans, Christoph Schied, and Alexander Keller. Instant neural graphics primitives with a multiresolution hash encoding. *ACM transactions on graphics (TOG)*, 41(4): 1–15, 2022.

[56] Richard A Newcombe, Steven J Lovegrove, and Andrew J Davison. Dtam: Dense tracking and mapping in real-time. In *2011 international conference on computer vision*, pages 2320–2327. IEEE, 2011.

[57] Sergio Orts-Escolano, Christoph Rhemann, Sean Fanello, Wayne Chang, Adarsh Kowdle, Yury Degtyarev, David Kim, Philip L Davidson, Sameh Khamis, Mingsong Dou, et al. Holoportation: Virtual 3d teleportation in real-time. In *Proceedings of the 29th annual symposium on user interface software and technology*, pages 741–754, 2016.

[58] Panagiotis Papantonakis, Georgios Kopanas, Bernhard Kerbl, Alexandre Lanvin, and George Drettakis. Reducing the memory footprint of 3d gaussian splatting. In *Proceedings of the ACM on Computer Graphics and Interactive Techniques*, volume 7, 2024.

[59] Keunhong Park, Utkarsh Sinha, Peter Hedman, Jonathan T. Barron, Sofien Bouaziz, Dan B Goldman, Ricardo Martin-Brualla, and Steven M. Seitz. Hypernerf: A higher-dimensional representation for topologically varying neural radiance fields. *ACM Trans. Graph.*, 40(6), dec 2021.

[60] Sergio Pissanetzky. *Sparse matrix technology-electronic edition*. Academic Press, 1984.

[61] Fabián Prada, Misha Kazhdan, Ming Chuang, Alvaro Collet, and Hugues Hoppe. Spatiotemporal atlas parameterization for evolving meshes. *ACM Transactions on Graphics (TOG)*, 36(4):1–12, 2017.

[62] Albert Pumarola, Enric Corona, Gerard Pons-Moll, and Francesc Moreno-Noguer. D-nerf: Neural radiance fields for dynamic scenes. In *Proceedings of the IEEE/CVF Conference on Computer Vision and Pattern Recognition*, pages 10318–10327, 2021.

[63] Shenhan Qian, Tobias Kirschstein, Liam Schoneveld, Davide Davoli, Simon Giebenhain, and Matthias Nießner. Gaussianavatars: Photorealistic head avatars with rigged 3d gaussians. *arXiv preprint arXiv:2312.02069*, 2023.

[64] René Ranftl, Katrin Lasinger, David Hafner, Konrad Schindler, and Vladlen Koltun. Towards robust monocular depth estimation: Mixing datasets for zero-shot cross-dataset transfer. *IEEE Transactions on Pattern Analysis and Machine Intelligence*, 44(3), 2022.

[65] Umme Sara, Morium Akter, and Mohammad Shorif Uddin. Image quality assessment through fsim, ssim, mse and psnr—a comparative study. *Journal of Computer and Communications*, 7 (3):8–18, 2019.

[66] Ruizhi Shao, Zerong Zheng, Hanzhang Tu, Boning Liu, Hongwen Zhang, and Yebin Liu. Tensor4d: Efficient neural 4d decomposition for high-fidelity dynamic reconstruction and rendering. In *Proceedings of the IEEE/CVF Conference on Computer Vision and Pattern Recognition*, pages 16632–16642, 2023.

[67] Vincent Sitzmann, Justus Thies, Felix Heide, Matthias Nießner, Gordon Wetzstein, and Michael Zollhofer. Deepvoxels: Learning persistent 3d feature embeddings. In *Proceedings of the IEEE Conference on Computer Vision and Pattern Recognition*, pages 2437–2446, 2019.

[68] Liangchen Song, Anpei Chen, Zhong Li, Zhang Chen, Lele Chen, Junsong Yuan, Yi Xu, and Andreas Geiger. Nerfplayer: A streamable dynamic scene representation with decomposed neural radiance fields. *IEEE Transactions on Visualization and Computer Graphics*, 29(5): 2732–2742, 2023. doi: 10.1109/TVCG.2023.3247082.

[69] Jiakai Sun, Han Jiao, Guangyuan Li, Zhanjie Zhang, Lei Zhao, and Wei Xing. 3dgstream: On-the-fly training of 3d gaussians for efficient streaming of photo-realistic free-viewpoint videos. *arXiv preprint arXiv:2403.01444*, 2024.

[70] Towaki Takikawa, Alex Evans, Jonathan Tremblay, Thomas Müller, Morgan McGuire, Alec Jacobson, and Sanja Fidler. Variable bitrate neural fields. In *ACM SIGGRAPH 2022 Conference Proceedings*, pages 1–9, 2022.

[71] Jiaxiang Tang, Xiaokang Chen, Jingbo Wang, and Gang Zeng. Compressible-composable nerf via rank-residual decomposition. *Advances in Neural Information Processing Systems*, 35: 14798–14809, 2022.

[72] Ayush Tewari, Justus Thies, Ben Mildenhall, Pratul Srinivasan, Edgar Tretschk, Wang Yifan, Christoph Lassner, Vincent Sitzmann, Ricardo Martin-Brualla, Stephen Lombardi, et al. Advances in neural rendering. In *Computer Graphics Forum*, volume 41, pages 703–735. Wiley Online Library, 2022.

[73] Edgar Tretschk, Ayush Tewari, Vladislav Golyanik, Michael Zollhöfer, Christoph Lassner, and Christian Theobalt. Non-rigid neural radiance fields: Reconstruction and novel view synthesis of a dynamic scene from monocular video. In *IEEE International Conference on Computer Vision (ICCV)*. IEEE, 2021.

[74] Edith Tretschk, Vladislav Golyanik, Michael Zollhöfer, Aljaz Bozic, Christoph Lassner, and Christian Theobalt. Scenerflow: Time-consistent reconstruction of general dynamic scenes. In *International Conference on 3D Vision (3DV)*, 2024.

[75] Chaoyang Wang, Ben Eckart, Simon Lucey, and Orazio Gallo. Neural trajectory fields for dynamic novel view synthesis. *arXiv preprint arXiv:2105.05994*, 2021.

[76] Feng Wang, Sinan Tan, Xinghang Li, Zeyue Tian, Yafei Song, and Huaping Liu. Mixed neural voxels for fast multi-view video synthesis. In *Proceedings of the IEEE/CVF International Conference on Computer Vision*, pages 19706–19716, 2023.

[77] Liao Wang, Jiakai Zhang, Xinhang Liu, Fuqiang Zhao, Yanshun Zhang, Yingliang Zhang, Minye Wu, Jingyi Yu, and Lan Xu. Fourier plenoctrees for dynamic radiance field rendering in real-time. In *Proceedings of the IEEE/CVF Conference on Computer Vision and Pattern Recognition*, pages 13524–13534, 2022.

[78] Liao Wang, Qiang Hu, Qihan He, Ziyu Wang, Jingyi Yu, Tinne Tuytelaars, Lan Xu, and Minye Wu. Neural residual radiance fields for streamably free-viewpoint videos. In *Proceedings of the IEEE/CVF Conference on Computer Vision and Pattern Recognition (CVPR)*, pages 76–87, June 2023.

[79] Liao Wang, Qiang Hu, Qihan He, Ziyu Wang, Jingyi Yu, Tinne Tuytelaars, Lan Xu, and Minye Wu. Neural residual radiance fields for streamably free-viewpoint videos. In *Proceedings of the IEEE/CVF Conference on Computer Vision and Pattern Recognition*, pages 76–87, 2023.

[80] Liao Wang, Kaixin Yao, Chengcheng Guo, Zhirui Zhang, Qiang Hu, Jingyi Yu, Lan Xu, and Minye Wu. Videorf: Rendering dynamic radiance fields as 2d feature video streams, 2023.

[81] Qianqian Wang, Yen-Yu Chang, Ruojin Cai, Zhengqi Li, Bharath Hariharan, Aleksander Holynski, and Noah Snavely. Tracking everything everywhere all at once. In *International Conference on Computer Vision*, 2023.

[82] Shengze Wang, Alexey Supikov, Joshua Ratcliff, Henry Fuchs, and Ronald Azuma. Inv: Towards streaming incremental neural videos. *arXiv preprint arXiv:2302.01532*, 2023.

[83] Chung-Yi Weng, Brian Curless, Pratul P Srinivasan, Jonathan T Barron, and Ira Kemelmacher-Shlizerman. Humannerf: Free-viewpoint rendering of moving people from monocular video. In *Proceedings of the IEEE/CVF conference on computer vision and pattern Recognition*, pages 16210–16220, 2022.

[84] Guanjun Wu, Taoran Yi, Jiemin Fang, Lingxi Xie, Xiaopeng Zhang, Wei Wei, Wenyu Liu, Qi Tian, and Wang Xinggang. 4d gaussian splatting for real-time dynamic scene rendering. In *Proceedings of the IEEE/CVF Conference on Computer Vision and Pattern Recognition*, 2024.

[85] Minye Wu, Zehao Wang, Georgios Kouros, and Tinne Tuytelaars. Tetrirf: Temporal tri-plane radiance fields for efficient free-viewpoint video. In *Proceedings of the IEEE/CVF conference on computer vision and pattern recognition*, 2024.

[86] Wenqi Xian, Jia-Bin Huang, Johannes Kopf, and Changil Kim. Space-time neural irradiance fields for free-viewpoint video. In *Proceedings of the IEEE/CVF Conference on Computer Vision and Pattern Recognition*, pages 9421–9431, 2021.

[87] Yiheng Xie, Towaki Takikawa, Shunsuke Saito, Or Litany, Shiqin Yan, Numair Khan, Federico Tombari, James Tompkin, Vincent Sitzmann, and Srinath Sridhar. Neural fields in visual computing and beyond. In *Computer Graphics Forum*, volume 41, pages 641–676. Wiley Online Library, 2022.

[88] Zhen Xu, Sida Peng, Haotong Lin, Guangzhao He, Jiaming Sun, Yujun Shen, Hujun Bao, and Xiaowei Zhou. 4k4d: Real-time 4d view synthesis at 4k resolution. *arXiv preprint arXiv:2310.11448*, 2023.

[89] Zeyu Yang, Hongye Yang, Zijie Pan, and Li Zhang. Real-time photorealistic dynamic scene representation and rendering with 4d gaussian splatting. In *International Conference on Learning Representations (ICLR)*, 2024.

[90] Ziyi Yang, Xinyu Gao, Wen Zhou, Shaohui Jiao, Yuqing Zhang, and Xiaogang Jin. Deformable 3d gaussians for high-fidelity monocular dynamic scene reconstruction. *arXiv preprint arXiv:2309.13101*, 2023.

[91] Yao Yao, Zixin Luo, Shiwei Li, Tian Fang, and Long Quan. Mvsnet: Depth inference for unstructured multi-view stereo. In *Proceedings of the European conference on computer vision (ECCV)*, pages 767–783, 2018.

[92] Alex Yu, Ruilong Li, Matthew Tancik, Hao Li, Ren Ng, and Angjoo Kanazawa. Plenoctrees for real-time rendering of neural radiance fields. In *Proceedings of the IEEE/CVF International Conference on Computer Vision*, pages 5752–5761, 2021.

[93] Raza Yunus, Jan Eric Lenssen, Michael Niemeyer, Yiyi Liao, Christian Rupprecht, Christian Theobalt, Gerard Pons-Moll, Jia-Bin Huang, Vladislav Golyanik, and Eddy Ilg. Recent trends in 3d reconstruction of general non-rigid scenes. In *Computer Graphics Forum*, page e15062. Wiley Online Library, 2024.

[94] Jiakai Zhang, Liao Wang, Xinhang Liu, Fuqiang Zhao, Minzhang Li, Haizhao Dai, Boyuan Zhang, Wei Yang, Lan Xu, and Jingyi Yu. Neuvv: Neural volumetric videos with immersive rendering and editing. *arXiv preprint arXiv:2202.06088*, 2022.

[95] Fuqiang Zhao, Wei Yang, Jiakai Zhang, Pei Lin, Yingliang Zhang, Jingyi Yu, and Lan Xu. Humannerf: Efficiently generated human radiance field from sparse inputs. In *Proceedings of the IEEE/CVF Conference on Computer Vision and Pattern Recognition (CVPR)*, pages 7743–7753, June 2022.

[96] C Lawrence Zitnick, Sing Bing Kang, Matthew Uyttendaele, Simon Winder, and Richard Szeliski. High-quality video view interpolation using a layered representation. *ACM transactions on graphics (TOG)*, 23(3):600–608, 2004.

[97] Matthias Zwicker, Hanspeter Pfister, Jeroen Van Baar, and Markus Gross. Surface splatting. In *Proceedings of the 28th annual conference on Computer graphics and interactive techniques*, pages 371–378, 2001.

Appendix

We provide supplementary results (Appendix A), additional implementation details (Appendix B), discussion on limitations and future work (Appendix C) and the broader impact (Appendix D) of our approach. We recommend the reader to watch the supplementary video hosted on our project website: `https://research.nvidia.com/labs/amri/projects/queen` for a visual comparison of the results of the various methods as well as more details of this project.

A Supplementary Results

A.1 Quantization vs. Gating

We evaluate the effect of the gating framework in comparison to the quantization framework for the position residuals. We perform gating or quantization on the position residuals while quantizing all other attributes. Results, averaged on the N3DV dataset, are shown in Figure 7. We vary training epochs per frame from 6 to 15 for gating and 6 to 25 for quantization to obtain trade-off curves. Increased training epochs result in higher reconstruction quality (PSNR) but longer training time or a larger model size. The left figure shows the PSNR versus size tradeoff while the right figure shows PSNR versus training time tradeoff. We see that, in both cases, the gating framework produces much better tradeoff curves than quantization, with PSNR values more than 0.2dB higher at similar sizes. When increasing the number of training iterations, quantization still improves in quality albeit at a slower rate requiring more training iterations for convergence. This demonstrates that position attributes are more sensitive to quantization errors and require full precision. It justifies our choice of learning to sparsify them as opposed to quantizing them. However, this does not translate to the other geometric attributes, scaling and rotation, where quantization is sufficient in compressing the attributes. This is seen in the results in Table 5 on the Exhibit scene from the Immersive dataset. Quantizing both rotation and scaling results in the lowest storage memory per frame at a similar PSNR and slightly higher training time.

Table 5: Gating versus Quantization of Rotation and Scale Attributes

Rotation	Scaling	PSNR	Storage Mem (MB)	Training Time (s)
Quantization	Quantization	29.15	2.47	21.61
Gating	Quantization	29.26	3.62	20.44
Quantization	Gating	28.92	3.64	19.89

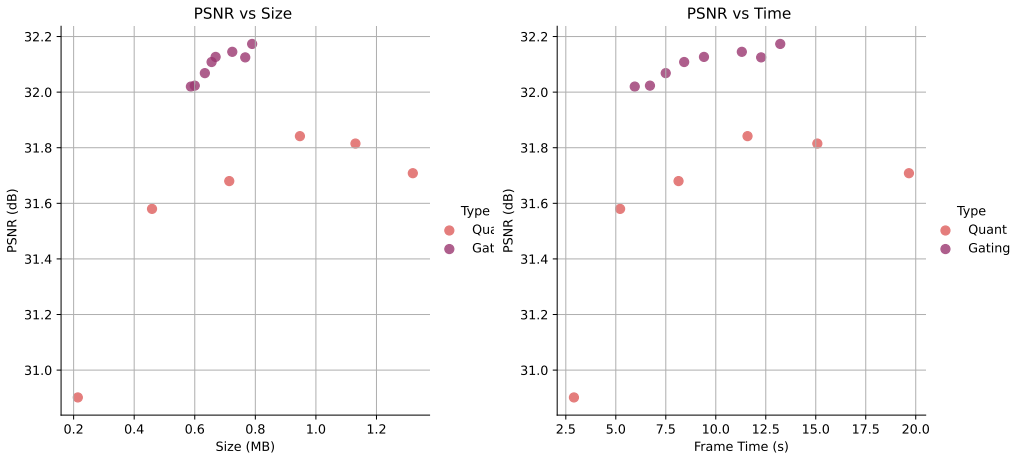

Figure 7: **Effect of Gating vs Quantization of Position Residuals.** Gating leads to much better PSNR versus size or PSNR versus training time tradeoff curves due to higher precision residuals.

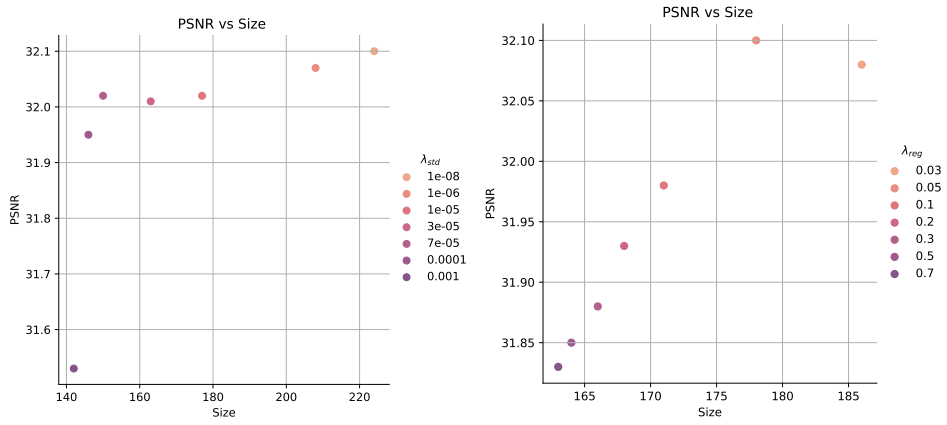

(a) (b)

Figure 8: **PSNR-Size Tradeoffs.** We evaluate the effect of varying λ_{std} and λ_{reg} for (a) the quantized latents and (b) the sparse position residuals. The storage size is measured in KB for the full video duration of 300 frames.

Table 6: **Effect of Latent Dimensions.** Dim is latent dimension and Size is total size of the 300-frame video in MB. *Metrics for Color SH are evaluated on three N3DV scenes.

Color SH*			Color Base			Rotation			Scaling		
Dim	PSNR	Size	Dim	PSNR	Size	Dim	PSNR	Size	Dim	PSNR	Size
1	33.69	155	2	32.02	211	2	32.00	182	2	32.13	215
2	33.73	157	4	32.04	211	4	31.98	183	4	32.06	219
4	33.78	156	8	32.04	213	6	32.01	182	8	32.11	224
8	33.71	156	12	32.06	215	8	32.00	182	12	32.07	226

A.2 Accuracy-memory Tradeoff

We consider the effect of varying different loss coefficients to trade off between accuracy and memory. In Figure 7 we explore the tradeoff between PSNR and size by varying the number of training iterations. We can also control the amount of sparsity in the scene by varying the λ_{reg} loss coefficient. As visualized in Fig. 8 (b), we find that increasing λ_{reg} leads to higher sparsity or lower memory but also lower reconstruction quality.

We further experiment with an additional regularization loss to reduce the entropy of the latents. We observe that lower entropy corresponds to lower memory, but also lower reconstruction quality. While learnable probability models can successfully reduce entropy, as shown by [25], these models have higher time and memory costs during training. We instead observe that the probability distribution of the various attribute residuals at each time-step is unimodal and is close to a Laplacian or Gaussian distribution. As a unimodal distribution has entropy proportional to the variance [11], we enforce a loss on the standard deviation of the latents with a tradeoff parameter λ_{std} controlling the effect of this regularization loss. Fig. 8(a) shows results on the N3DV dataset by varying λ_{std}. We observe that increasing λ_{std} reduces the entropy costs, leading to lower memory costs, but lower reconstruction quality, and vice versa.

A.3 Effect of Quantization Latent Dimension

We provide additional analysis on the effect of latent dimension for the various attributes in Table 6. In general, latent dimension does not have a significant effect on reconstruction quality or model size. Increasing the latent dimension can lead to lower per-dimension entropy due to our learnable quantization framework and hence still maintains the overall total size for the latent. We find that varying the total number of iterations (Appendix A.1) or the entropy loss/variance coefficient (Appendix A.2) are more effective knobs for trading off between quality-memory or quality-time.

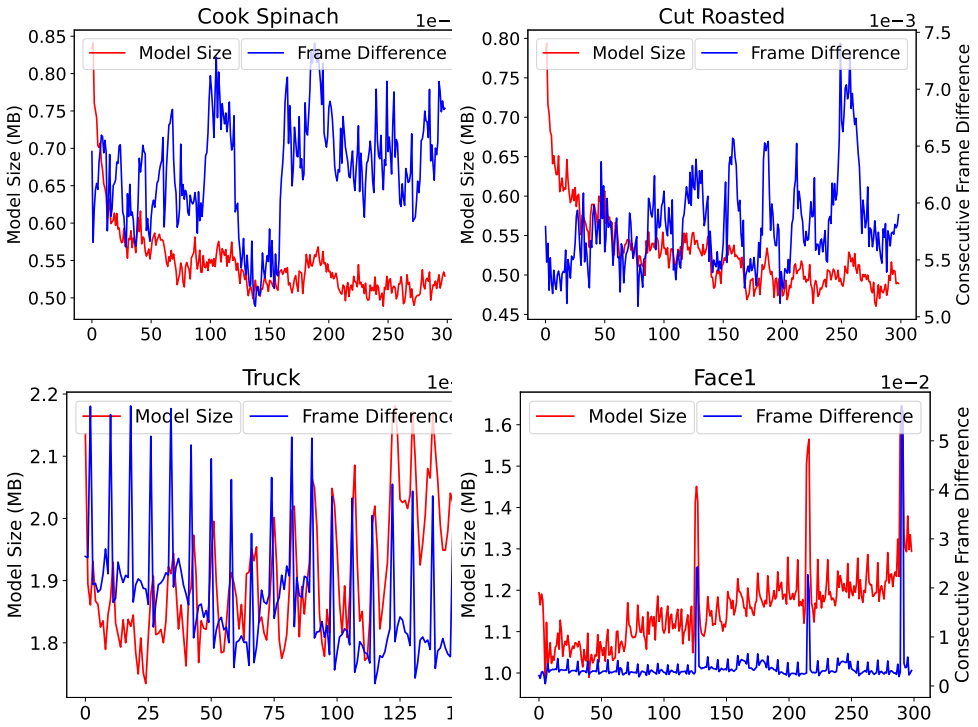

Figure 9: **Adaptive Sizes.** Our quantization-sparsity framework automatically allocates more memory for frames with larger scene changes (higher frame difference). Notice that the frame difference spikes in the Immersive scenes (bottom row) correlate with frame-wise model size, which increases to allow for modeling of more temporal variations.

A.4 Framewise PSNR and Size

A key advantage of our quantization-sparsity framework is its adaptability to scene content. We visualize the per frame sizes for 2 scenes each from N3DV and Immersive along with the visual frame difference between consecutive frames in Figure 9. We see that our approach allocates variable model sizes for each frame unlike 3DGStream [69], which uses a fixed-sized InstantNGP structure. Additionally, higher frame differences result in larger model sizes and vice versa, as seen in the top row. This shows that our method is capable of allocating more bits to frames with large scene changes. This is especially evident from the spikes in Immersive's scenes in the bottom row, which correlate with the model size.

Next, we show the stability of our approach at recovering from large scene variations corresponding to the frame difference spikes as mentioned above. We visualize the reconstructed test-view PSNR for each frame, for 2 scenes each from N3DV and Immersive, along with the frame difference between consecutive frames in Figure 10. A large L1 error such as around frames 175 (top left), frames 225 (top right), frames 75 (bottom left) or frames 90 and 290 (bottom right) does lead to drops in PSNR. However, our PSNR recovers in subsequent frames showing the stability of our framework with large scene variations present.

A.5 Effect of Improved Point Cloud Initialization.

Consistent geometry for the 3D scene in the first frame is important to learn accurate residuals for the attributes of the subsequent frames. The COLMAP-generated point cloud initialization can be incomplete for regions that are textureless or are not sufficiently captured in multiple cameras. This is visualized in the top row of Figure 11. The boundaries of the scene consist of limited training view cameras as shown by the white box leading to sparse or no points in these regions by COLMAP initialization. The densification stage in 3DGS is unable to recover from this producing erroneous rendered depth or geometry and also leads to low quality image reconstruction.

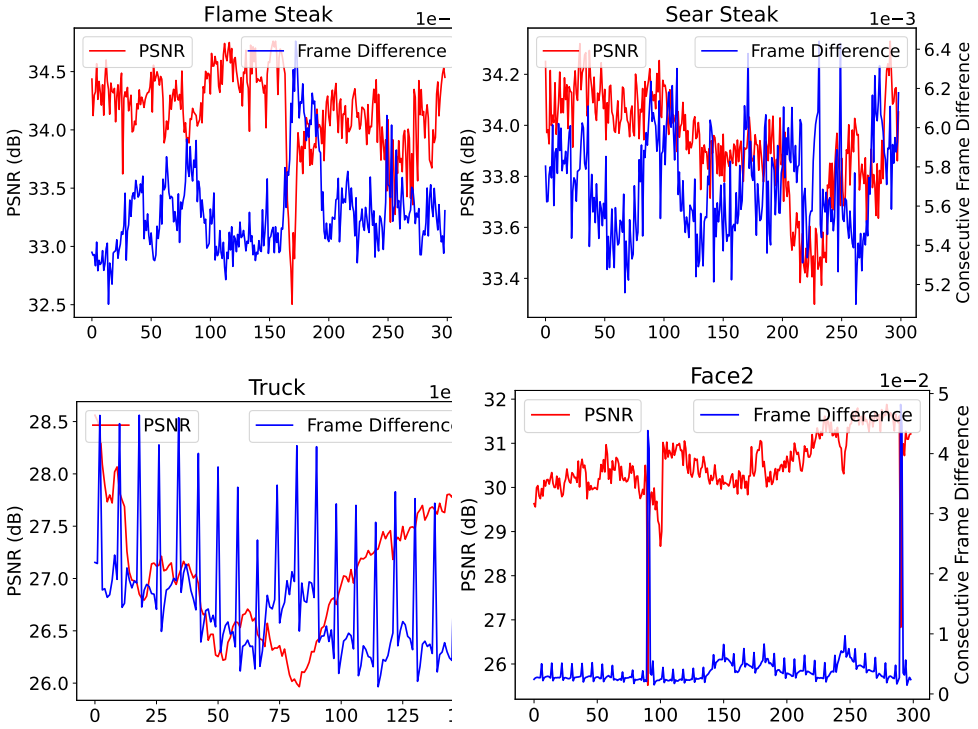

Figure 10: **Per-frame Quality Evaluation.** Our approach results in higher PSNR for large scene changes corresponding to higher consecutive frame difference such as around frame 175 (top right) or the spikes in the bottom right scene.

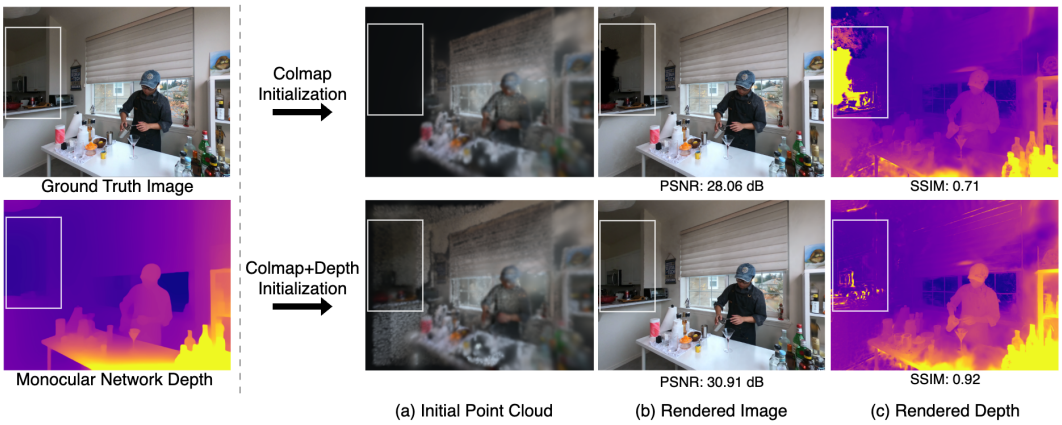

Figure 11: **Effect of Depth Initialization.** Top row: (a) COLMAP produces sparse or no points for regions of the scene with limited texture, producing (b) erroneous image rendering and (c) incorrect geometry or depth. Bottom row: initializing with depth maps predicted by an off-the-shelf monocular depth network produces better reconstruction and consistent scene geometry.

Therefore, we propose to use an off-the-shelf monocular depth estimation network [64] to predict a more complete initial point cloud. However, due to the scale-shift ambiguity of monocular depth estimation, we align the predicted monocular depth with the true scene depth from existing COLMAP points. To do so, we estimate the 2D pixel locations $\mathbf{p}'_i$ of each COLMAP point i by projecting points from 3D world space to 2D screenspace.

$$\mathbf{p}'_i = \Pi(\mathbf{p}_i; \mathbf{K}, \mathbf{W}), \tag{12}$$

where $\Pi(.)$ denotes the perspective transform described in Eq. 1 of the paper. We then query the pixel locations $\mathbf{p}'_i$ in the monocular depth image to obtain the corresponding depth values $\hat{z}_i$. This is

Table 7: **Effect of Depth Initialization on N3DV and Immersive datasets.**

Dataset	Initialization	PSNR (Test) (dB)↑	PSNR (Train) (dB)↑	Num. Points (in Millions) ↓	Training Time (s) ↓
N3DV	COLMAP	32.02	30.06	3.24	**13.24**
	+Depth	**32.03**	**31.42**	**3.14**	13.40
Immersive	COLMAP	28.52	32.38	**3.10**	**18.62**
	+Depth	**29.10**	**32.65**	3.21	18.91

aligned with the GT depth value from the COLMAP 3D points z_i by a least-squares optimization to obtain the scale and shift parameters α, β. We then obtain the aligned dense depth map $\alpha\hat{z}_i + \beta$.

To identify regions with empty COLMAP initializations, we iterate over training views and render the corresponding image along with an alpha mask calculating the accumulated transmittance at each pixel location. Mask values below a threshold t_z (0.10 for N3DV and 0.03 for Immersive) are identified to obtain the corresponding pixel locations containing few COLMAP points. We then use the aligned depth values corresponding to these pixel locations to re-project back into the world space.

As seen in the bottom row of Figure 11, the depth map initialization produces more dense points in empty regions. These points maintain consistent depth with existing COLMAP points. Such an initialization results in improved image reconstruction quality with $\sim$3dB improvement in PSNR for the corresponding view while also producing better consistent depth or geometry. As we utilize the network depth at initialization only, we do not require high-quality depth networks and a coarse depth is sufficient for sampling new points. The training can then learn to move the Gaussians to produce finer scene depth. This also results in minimal increases in training time as it's a one-time operation at the initial time-step and produces a small number of additional points in empty regions.

We show quantitative results for 2 configurations with and without depth map initialization for the datasets of N3DV and Immersive in Tab. 7. We show PSNR for the central test view as well as for the first train view for all scenes. We also show the number of points at the end of training the first frame with and without initialization along with the average training time per frame for the full scene. The depth initialization does not significantly affect the test view PSNR on N3DV as it corresponds to the central view with a large overlap with many training views. In contrast, the PSNR for the training view (also in Fig. 11) improves considerably (+1.3dB) with the depth initialization highlighting the efficacy of the approach in improving geometry for regions with sparse camera views. Additionally, there is almost no overhead cost as we obtain similar number of Gaussian points at the end of training the first frame. Training time for the full video is also only marginally higher. On Immersive, we observe a 0.5 dB improvement in PSNR for the test view while the train view PSNR shows minor improvements. Again, the number of Gaussians and training time is not significantly affected by the initialization with additional depth based points.

A.6 Additional Baseline Comparisons

We show comparisons to additional offline FVV baselines on the N3DV dataset in Table 8 for the sake of completeness. This is a superset of the Tab. 2 in the main paper. A majority of the works compute SSIM using the scikit-image implementation, which tends to produce higher values different from our SSIM implementation similar to MipNeRF [2]. Since the two are not comparable, we exclude implementation numbers computed with scikit-image. We also only show results for LPIPS on VGG for the methods that use it. This is consistent with how we compute LPIPS.

Table 8: **Quantitative Comparisons on the N3DV [41] and Immersive [4] Datasets.** We compare QUEEN against state-of-the-art online and include offline FVV methods for completeness. 3DGStream* refers to our re-implementation on the same NVIDIA A100 GPU as used by QUEEN for fairness. † is evaluated on the *flame salmon* scene only. Bold and underlined numbers indicate the **best** and the second best results, respectively, within each category.

Type	Method	PSNR (dB) ↑	SSIM ↑	LPIPS ↓	Storage (MB) ↓	Training (sec) ↓	Rendering (FPS) ↑
Offline	DyNeRF [41]	29.58†	0.961†	0.083†	**0.1**	15600	0.02
	NeRFPlayer [68]	30.69	0.932	0.209	17.1	72	0.05
	HyperReel [1]	31.10	0.928	-	1.2	104	2.00
	HexPlanes [5]	31.70	-	-	0.8	144	0.21
	K-Planes [19]	31.63	-	-	1.0	48	0.15
	MixVoxels [76]	31.34	-	-	1.7	16	38
	4DGS [89]	32.01	-	-	-	-	114
	HexPlanes-4DGS [84]	31.15	-	-	0.3	**6**	30
	SpaceTime [42]	**32.05**	**0.948**	-	0.67	20	**140**
Online	StreamRF [37]	30.68	-	-	31.4	15	8.3
	TeTriRF [85]	30.43	0.906	0.248	**0.06**	39	4
	3DGStream [69]	31.67	-	-	7.83	12	215
	3DGStream* [69]	31.58	0.941	0.140	7.80	8.5	261
	QUEEN-s	31.89	0.945	0.139	0.68	**4.65**	**345**
	QUEEN-m	32.03	0.946	0.137	0.69	5.96	321
	QUEEN-l	**32.19**	**0.946**	**0.136**	0.75	7.9	248

A.7 Per-scene Results

In addition to the average quantitative results over the full datasets of N3DV and Immersive in Tab. 8, we show results for each scene in both the N3DV and Immersive datasets of various frame-wise metrics, including, PSNR, SSIM, LPIPS, size, training time and rendering time (FPS) in Tables 9 and 10.

A.8 Perceptual quality: User study

In addition to the extensive quantitative analysis in the paper as well as supplementary, we conduct an A/B user study to measure the perceptual quality of our video reconstructions. For each vote, we show a pair of randomly chosen rendering results (from a test view that is not used in training) by our method and one of the baseline methods (3DGStream [69] and TeTriRF [85]). We also show the ground truth video as a reference for the participants to make the decision. We ask the participant to choose the method that more faithfully matches the reference video. In total, we collected 285 responses from 15 participants within the timeline of the rebuttal. For the N3DV dataset, 76.67% of users preferred our method over 3DGStream and 96.67% preferred our method over TeTriRF. On the Google Immersive dataset, 97.14% of users preferred the reconstructions from our approach over that of 3DGStream. This showed that the participants strongly prefer our results in comparison to the baseline methods for both datasets.

B Implementation Details

Training. Our implementation of QUEEN builds on that of [29]. We train the Gaussians for 500 and 350 epochs for first time-step, and for 10 and 15 epochs for the subsequent time-steps, on N3DV and Immersive, respectively, with each epoch consisting of all training views. We set the SH degree to 2 for N3DV and 3 for Immersive. We set the score vector threshold $t_{\mathbf{d}} = 0.001$ for all experiments. We additionally dilate the image mask by a 48×48 kernel to include neighboring image regions while rendering as larger Gaussians can depend on multiple pixel locations. We perform masked training for 30% of the iterations for N3DV and 65% for Immersive. We perform masked training for only a fraction of iterations as updating Gaussians rendered only at masked locations can alter the rendered pixels at unmasked location as well. We thus allow fine-tuning on the full image to account for any changes in the unmasked image regions.

Table 9: **Per-scene Metrics for the N3DV Datasets**

Scene	PSNR (dB) ↑	SSIM ↑	LPIPS ↓	Storage (MB) ↓	Training (sec) ↓	Rendering (FPS) ↑
Coffee Martini	28.38	0.915	0.155	1.17	7.48	213
Cook Spinach	33.4	0.956	0.134	0.59	8.03	254
Cut Beef	34.01	0.959	0.132	0.57	7.59	291
Sear Steak	33.93	0.962	0.125	0.56	9.31	257
Flame Steak	34.17	0.962	0.126	0.59	7.97	266
Flame Salmon	29.25	0.923	0.145	1.00	7.00	207
Average	32.19	0.946	0.136	0.75	7.90	248

Table 10: **Per-scene Metrics for the Immersive Datasets**

Scene	PSNR (dB) ↑	SSIM ↑	LPIPS ↓	Storage (MB) ↓	Training (sec) ↓	Rendering (FPS) ↑
Welder	27.03	0.884	0.215	2.18	18.23	146
Flames	30.52	0.925	0.157	1.26	29.54	161
Truck	27.03	0.905	0.195	2.03	17.12	177
Exhibit	28.03	0.903	0.193	2.11	17.81	170
Face Paint 1	31.90	0.950	0.240	1.19	17.48	245
Face Paint 2	30.55	0.937	0.207	2.39	17.49	217
Cave	29.49	0.900	0.250	1.50	20.46	162
Average	29.22	0.915	0.208	1.79	19.73	183

Sparse Gating. We learn the parameters α with the Adam optimizer [30]. The position residual learning rate is set to 0.00016 for N3DV and 0.0005 for Immersive. Other hyperparameters are provided in Table 11.

Quantization. For both datasets, we set the learning rate of the decoder parameters to be 0.001 for the color and rotation attributes and 0.0001 for opacity and scaling, optimized with the Adam optimizer. Other hyperparameters are provided in Table 12.

Densification. For N3DV, we perform densification for subsequent frames from epoch 6 until 80% of the epochs with an interval of 2 epochs and a gradient threshold of 0.00125. For Immersive, we perform densification on the 8th epoch with a gradient threshold of 0.00125.

Table 11: **Gating Hyperparameters**

Dataset	LR	λ_{reg}	γ_0	γ_1	τ
N3DV	0.1	0.01	-0.5	1.01	0.3
Immersive	0.1	0.01	-0.1	1.1	0.5

First-frame Quantization. Uncompressed Gaussians have large memory costs even for the first frame. However, quantizing all attributes results in quality degradations [24]. We therefore apply learnable quantization only on the first frame's high-frequency spherical harmonic coefficients (excluding the DC component) using the hyperparameters mentioned above. For example, on N3DV, we reduce the first frame's size from 47 to 17 MB with no quality degradation.

Storage. Post-training, we convert the learned parameters to the final compressed form. For the quantized residuals of rotation, scale, opacity and appearance, we convert the continuous latents $\mathbf{L}_c$ to the integer form and then apply entropy encoding and store this further-compressed representation $\mathbf{E}_c$ as well as the decoder $\mathbf{D}_c$ for all four categories $c \in \{\text{r, s, o, } \mathbf{h}\}$. Our entropy coding approach flattens our integer latent matrix for each attribute before encoding. For example, for L-dimensional latent attributes for N gaussians, we flatten the matrix to obtain a vector with L*N elements. This integer vector is then encoded using standard entropy coding approaches such as arithmetic coding.

Table 12: **Quantization Hyperparameters**

Dataset	Rotation		Scaling		Opacity		Color Base		Color Freq	
	Latent Dim	Latent LR	Latent Dim	Latent LR	Latent Dim	Latent LR	Latent Dim	Latent LR	Latent Dim	Latent LR
N3DV	6	0.025	8	0.01	3	0.05	8	0.0125	4	0.000625
Immersive	6	0.015	8	0.007	3	0.05	8	0.0125	12	0.000375

The number of bits for storing each attribute residual matrix is therefore dependent on the scene content as it relies on the amount of motion. This number can be fractional, on average, which is the standard for the entropy coding algorithm of arithmetic coding or Huffman coding [33]. For example, for the Sear Steak scene in the N3DV dataset, on average, we require 0.68 bits for all the quantized attributes (corresponding to 0.5MB/frame). This depends on the entropy of the latents itself, which varies with changing scene motion (Figure 9).

For the sparse gates, we store the positional residuals as a sparse matrix with the indices from binarized gate variables $\mathbf{I} = \{i | g_i \neq 0\}$, and the full-precision residual vectors only if its corresponding gate is on, $\mathbf{E}_p = \{\mathbf{l}_{p_i} | i \in I\}$. Both operations add a negligible computation overhead. This corresponds to the coordinate format (COO) for storing sparse matrices where the non-zero values are stored in FP-32 precision along with their integer index locations.

B.1 Sensitivity Analysis on Hyperparameter

Table 13: **Sensitivity to different hyperparameter configurations on the N3DV dataset.**

Method	PSNR	Size (MB)
Ours (N3DV hyperparam.)	32.14	0.60
Ours (Immersive hyperparam.)	32.06	1.49
3DGStream [69]	31.58	7.80

We set different hyperparameters for the two datasets in in Tables 11 and 12 to account for the widely varying amount of scene motion between N3DV and Immersive datasets. The Immersive dataset contains larger and more complex scene motions (e.g., a person entering and leaving the scene) while N3DV contains relatively minor motions. We found that a higher learning rate for the position residuals allows Gaussians to adapt to the highly dynamic scenes. The gating hyperparameters in Table 11 for N3DV are set to utilize this prior information about the dataset where the stretch hyperparameters γ_0 and γ_1 are set closer to 0 to enforce more sparsity in the position residuals. Additionally, the Immersive dataset itself consists of a wide variety of indoor/outdoor scenes at varying scales/scene motion/illumination. We use the same set of hyperparameters for each scene achieving good reconstruction quality for every scene (Table 10) showing its generalization capability.

Tables 11 and 12 list out the different hyperparameters for quantizing and sparsifying residuals for both N3DV and Immersive datasets. To test the sensitivity of reconstruction quality to hyperparameters, we train our method on the N3DV dataset with two sets of hyperparameters. The first configuration uses the stated hyperparameters for N3DV from Tables 11 and 12, while the second utilizes the hyperparameters corresponding to Immersive while also matching the learning rate for the position residuals (0.0005). We show results on N3DV datasets in Table 13. We see that the Immersive dataset's hyperparameter configuration still achieves similar PSNR as the original hyperparameters for N3DV. While the model size is higher (1.49 MB) with the Immersive configuration compared to the original configuration (0.60 MB), it is still much lower than the prior state-of-the-art 3DGStream (7.8 MB) while maintaining higher reconstruction quality in terms of PSNR.

B.2 Evaluation

Datasets. (1) Neural 3D Video (N3DV) Datasets [41] consist of six indoor scenes with forward-facing multiview videos with up to 20 cameras at 2704×2028 resolution. Similar to prior work, we downsample videos by a factor of 2 for training and testing, holding out the central view for testing. Each video consists of 300 frames at 30 FPS. **(2) Immersive Video Datasets** [4] consist of light field videos of indoor and outdoor scenes captured using a 46-camera rig with fisheye lenses. Following

prior work, we downsample videos by a factor of 2 to obtain a resolution of 1280×960. We evaluate on 7 scenes (Welder, Flames, Truck, Exhibit, Face Paint 1, Face Paint 2 and Cave) with the central view held out for testing. We extract the first 300 frames for all scenes except for Truck, which consists of 150 frames. We undistort the fisheye views into perspective views using the distortion parameters. We train and evaluate on the perspective views with pinhole camera parameters.

Baselines. 3DGStream [69]: We use the official codebase[4] from 3DGStream [69]. We use the same default configuration for N3DV as provided by the authors. For Immersive, we reduce the gradient threshold for densification to 0.0075 to allow for more Gaussians while increasing the training iterations for Stage 1 and 2 to be 450 and 250 iterations, respectively. **TeTriRF [85]:** We use the official codebase[5] from TeTriRF [85] for all experiments on N3DV.

Measuring FPS. We compute FPS for all frames of the video and report the median value in our experiments including the time taken to decode the residuals. Note that the decoding is a one-time operation per step and rendering for a preceding frame can be performed while learning the residuals of a subsequent ones to achieve even higher speeds.

C Limitations and Future Work

For efficiency and on-the-fly training, we encode sequences by learning inter-frame residuals. However, for FVVs of long duration or drastic scene update, per-frame training will face challenges in reconstruction capability. Unlike offline reconstruction, per-frame training does not have access to future-frame information. This setup limits the capability to effectively reason about large scene changes (e.g., topological changes and highly varying appearance) [56]. If an object suddenly appears or disappears, it is more difficult to (de-)allocate and update scene parameters to capture such changes. In the context of Gaussian splatting, it is challenging to schedule densification and pruning of the Gaussians. Future work could address this by designing an efficient keyframing technique for identifying large changes in the scene and allocate longer training times accordingly.

Furthermore, most current FVV encoding paradigms rely on the input multi-view videos for reconstruction. Exploring a general prior of the dynamic scenes, e.g., generative video models, is a promising direction for reducing the dependence on coherent multi-view input, as the video prior could regularize the reconstructed FVV to capture reasonable scene dynamics even if some input views or frames are missing. Moreover, extending our approach to a single or sparse view scenario is a challenging yet important problem for further democratizing streamable FVV. We will leave these directions for future work.

D Broader Impacts

We consider our work as a neutral technology. This proposed method reconstructs free-viewpoint videos from user-provided video inputs. As we highlighted in the introduction, this technology can improve many aspect of people's lives, such as through healthcare (tele-operation) and communications (3D video conferencing). There is indeed a possibility that this work can be misused. Since our reconstruction completely relies on the video inputs, the most likely cases of misuse are those where the input video (provided by the users) have negative impacts.

[4] https://github.com/SJoJoK/3DGStream

[5] https://github.com/wuminye/TeTriRF

NeurIPS Paper Checklist

1. **Claims**

   Question: Do the main claims made in the abstract and introduction accurately reflect the paper's contributions and scope?

   Answer: [Yes]

   Justification: We show extensive experiments and ablations on multiple datasets which are widely used in the area. Our claims accurately reflect the contribution and scope of our work.

   Guidelines:

   - The answer NA means that the abstract and introduction do not include the claims made in the paper.
   - The abstract and/or introduction should clearly state the claims made, including the contributions made in the paper and important assumptions and limitations. A No or NA answer to this question will not be perceived well by the reviewers.
   - The claims made should match theoretical and experimental results, and reflect how much the results can be expected to generalize to other settings.
   - It is fine to include aspirational goals as motivation as long as it is clear that these goals are not attained by the paper.

2. **Limitations**

   Question: Does the paper discuss the limitations of the work performed by the authors?

   Answer: [Yes]

   Justification: We discuss limitations of our work in our conclusions section. We add further detail on several limitations of our work in Appendix C.

   Guidelines:

   - The answer NA means that the paper has no limitation while the answer No means that the paper has limitations, but those are not discussed in the paper.
   - The authors are encouraged to create a separate "Limitations" section in their paper.
   - The paper should point out any strong assumptions and how robust the results are to violations of these assumptions (e.g., independence assumptions, noiseless settings, model well-specification, asymptotic approximations only holding locally). The authors should reflect on how these assumptions might be violated in practice and what the implications would be.
   - The authors should reflect on the scope of the claims made, e.g., if the approach was only tested on a few datasets or with a few runs. In general, empirical results often depend on implicit assumptions, which should be articulated.
   - The authors should reflect on the factors that influence the performance of the approach. For example, a facial recognition algorithm may perform poorly when image resolution is low or images are taken in low lighting. Or a speech-to-text system might not be used reliably to provide closed captions for online lectures because it fails to handle technical jargon.
   - The authors should discuss the computational efficiency of the proposed algorithms and how they scale with dataset size.
   - If applicable, the authors should discuss possible limitations of their approach to address problems of privacy and fairness.
   - While the authors might fear that complete honesty about limitations might be used by reviewers as grounds for rejection, a worse outcome might be that reviewers discover limitations that aren't acknowledged in the paper. The authors should use their best judgment and recognize that individual actions in favor of transparency play an important role in developing norms that preserve the integrity of the community. Reviewers will be specifically instructed to not penalize honesty concerning limitations.

3. **Theory Assumptions and Proofs**

   Question: For each theoretical result, does the paper provide the full set of assumptions and a complete (and correct) proof?

Answer: [NA]

Justification: Our work is not a theory work. All equations for the various components of our work are explained in detail in Sec. 3, where we cited appropriate sources for their theoretical work in the related work and the method sections.

Guidelines:

- The answer NA means that the paper does not include theoretical results.
- All the theorems, formulas, and proofs in the paper should be numbered and cross-referenced.
- All assumptions should be clearly stated or referenced in the statement of any theorems.
- The proofs can either appear in the main paper or the supplemental material, but if they appear in the supplemental material, the authors are encouraged to provide a short proof sketch to provide intuition.
- Inversely, any informal proof provided in the core of the paper should be complemented by formal proofs provided in appendix or supplemental material.
- Theorems and Lemmas that the proof relies upon should be properly referenced.

4. **Experimental Result Reproducibility**

Question: Does the paper fully disclose all the information needed to reproduce the main experimental results of the paper to the extent that it affects the main claims and/or conclusions of the paper (regardless of whether the code and data are provided or not)?

Answer: [Yes]

Justification: We provide extensive explanations of each component of our work in detail in Sec. 3. Additional implementation details with corresponding hyperparameters are also provided in Appendix B.

Guidelines:

- The answer NA means that the paper does not include experiments.
- If the paper includes experiments, a No answer to this question will not be perceived well by the reviewers: Making the paper reproducible is important, regardless of whether the code and data are provided or not.
- If the contribution is a dataset and/or model, the authors should describe the steps taken to make their results reproducible or verifiable.
- Depending on the contribution, reproducibility can be accomplished in various ways. For example, if the contribution is a novel architecture, describing the architecture fully might suffice, or if the contribution is a specific model and empirical evaluation, it may be necessary to either make it possible for others to replicate the model with the same dataset, or provide access to the model. In general. releasing code and data is often one good way to accomplish this, but reproducibility can also be provided via detailed instructions for how to replicate the results, access to a hosted model (e.g., in the case of a large language model), releasing of a model checkpoint, or other means that are appropriate to the research performed.
- While NeurIPS does not require releasing code, the conference does require all submissions to provide some reasonable avenue for reproducibility, which may depend on the nature of the contribution. For example
  (a) If the contribution is primarily a new algorithm, the paper should make it clear how to reproduce that algorithm.
  (b) If the contribution is primarily a new model architecture, the paper should describe the architecture clearly and fully.
  (c) If the contribution is a new model (e.g., a large language model), then there should either be a way to access this model for reproducing the results or a way to reproduce the model (e.g., with an open-source dataset or instructions for how to construct the dataset).
  (d) We recognize that reproducibility may be tricky in some cases, in which case authors are welcome to describe the particular way they provide for reproducibility. In the case of closed-source models, it may be that access to the model is limited in some way (e.g., to registered users), but it should be possible for other researchers to have some path to reproducing or verifying the results.

5. **Open access to data and code**

   Question: Does the paper provide open access to the data and code, with sufficient instructions to faithfully reproduce the main experimental results, as described in supplemental material?

   Answer: [No]

   Justification: We aim to release the code in the future.

   Guidelines:

   - The answer NA means that paper does not include experiments requiring code.
   - Please see the NeurIPS code and data submission guidelines (`https://nips.cc/public/guides/CodeSubmissionPolicy`) for more details.
   - While we encourage the release of code and data, we understand that this might not be possible, so "No" is an acceptable answer. Papers cannot be rejected simply for not including code, unless this is central to the contribution (e.g., for a new open-source benchmark).
   - The instructions should contain the exact command and environment needed to run to reproduce the results. See the NeurIPS code and data submission guidelines (`https://nips.cc/public/guides/CodeSubmissionPolicy`) for more details.
   - The authors should provide instructions on data access and preparation, including how to access the raw data, preprocessed data, intermediate data, and generated data, etc.
   - The authors should provide scripts to reproduce all experimental results for the new proposed method and baselines. If only a subset of experiments are reproducible, they should state which ones are omitted from the script and why.
   - At submission time, to preserve anonymity, the authors should release anonymized versions (if applicable).
   - Providing as much information as possible in supplemental material (appended to the paper) is recommended, but including URLs to data and code is permitted.

6. **Experimental Setting/Details**

   Question: Does the paper specify all the training and test details (e.g., data splits, hyperparameters, how they were chosen, type of optimizer, etc.) necessary to understand the results?

   Answer: [Yes]

   Justification: We follow benchmark and evaluation protocols that are widely used by existing work in the area. Additional hyperparameters and experiment details are provided in the supplementary materials B.

   Guidelines:

   - The answer NA means that the paper does not include experiments.
   - The experimental setting should be presented in the core of the paper to a level of detail that is necessary to appreciate the results and make sense of them.
   - The full details can be provided either with the code, in appendix, or as supplemental material.

7. **Experiment Statistical Significance**

   Question: Does the paper report error bars suitably and correctly defined or other appropriate information about the statistical significance of the experiments?

   Answer: [No]

   Justification: We follow benchmark and evaluation protocols that are widely used by existing work in the area. To our knowledge, most of the existing work in this area do not provide statistical significance.

   Guidelines:

   - The answer NA means that the paper does not include experiments.
   - The authors should answer "Yes" if the results are accompanied by error bars, confidence intervals, or statistical significance tests, at least for the experiments that support the main claims of the paper.

- The factors of variability that the error bars are capturing should be clearly stated (for example, train/test split, initialization, random drawing of some parameter, or overall run with given experimental conditions).
- The method for calculating the error bars should be explained (closed form formula, call to a library function, bootstrap, etc.)
- The assumptions made should be given (e.g., Normally distributed errors).
- It should be clear whether the error bar is the standard deviation or the standard error of the mean.
- It is OK to report 1-sigma error bars, but one should state it. The authors should preferably report a 2-sigma error bar than state that they have a 96% CI, if the hypothesis of Normality of errors is not verified.
- For asymmetric distributions, the authors should be careful not to show in tables or figures symmetric error bars that would yield results that are out of range (e.g. negative error rates).
- If error bars are reported in tables or plots, The authors should explain in the text how they were calculated and reference the corresponding figures or tables in the text.

8. **Experiments Compute Resources**

   Question: For each experiment, does the paper provide sufficient information on the computer resources (type of compute workers, memory, time of execution) needed to reproduce the experiments?

   Answer: [Yes]

   Justification: We provide details including computational resources (hardware), training times and dataset specifications in the implementation details in the main paper and the appendix.

   Guidelines:

   - The answer NA means that the paper does not include experiments.
   - The paper should indicate the type of compute workers CPU or GPU, internal cluster, or cloud provider, including relevant memory and storage.
   - The paper should provide the amount of compute required for each of the individual experimental runs as well as estimate the total compute.
   - The paper should disclose whether the full research project required more compute than the experiments reported in the paper (e.g., preliminary or failed experiments that didn't make it into the paper).

9. **Code Of Ethics**

   Question: Does the research conducted in the paper conform, in every respect, with the NeurIPS Code of Ethics `https://neurips.cc/public/EthicsGuidelines`?

   Answer: [Yes]

   Justification: Yes, the research conducted in the paper conform, in every respect, with the NeurIPS Code of Ethics.

   Guidelines:

   - The answer NA means that the authors have not reviewed the NeurIPS Code of Ethics.
   - If the authors answer No, they should explain the special circumstances that require a deviation from the Code of Ethics.
   - The authors should make sure to preserve anonymity (e.g., if there is a special consideration due to laws or regulations in their jurisdiction).

10. **Broader Impacts**

    Question: Does the paper discuss both potential positive societal impacts and negative societal impacts of the work performed?

    Answer: [Yes]

    Justification: Please see Appendix D where we discuss the potential societal impacts.

    Guidelines:

- The answer NA means that there is no societal impact of the work performed.
- If the authors answer NA or No, they should explain why their work has no societal impact or why the paper does not address societal impact.
- Examples of negative societal impacts include potential malicious or unintended uses (e.g., disinformation, generating fake profiles, surveillance), fairness considerations (e.g., deployment of technologies that could make decisions that unfairly impact specific groups), privacy considerations, and security considerations.
- The conference expects that many papers will be foundational research and not tied to particular applications, let alone deployments. However, if there is a direct path to any negative applications, the authors should point it out. For example, it is legitimate to point out that an improvement in the quality of generative models could be used to generate deepfakes for disinformation. On the other hand, it is not needed to point out that a generic algorithm for optimizing neural networks could enable people to train models that generate Deepfakes faster.
- The authors should consider possible harms that could arise when the technology is being used as intended and functioning correctly, harms that could arise when the technology is being used as intended but gives incorrect results, and harms following from (intentional or unintentional) misuse of the technology.
- If there are negative societal impacts, the authors could also discuss possible mitigation strategies (e.g., gated release of models, providing defenses in addition to attacks, mechanisms for monitoring misuse, mechanisms to monitor how a system learns from feedback over time, improving the efficiency and accessibility of ML).

11. **Safeguards**

    Question: Does the paper describe safeguards that have been put in place for responsible release of data or models that have a high risk for misuse (e.g., pretrained language models, image generators, or scraped datasets)?

    Answer: [NA]

    Justification: The paper poses no such risks.

    Guidelines:

    - The answer NA means that the paper poses no such risks.
    - Released models that have a high risk for misuse or dual-use should be released with necessary safeguards to allow for controlled use of the model, for example by requiring that users adhere to usage guidelines or restrictions to access the model or implementing safety filters.
    - Datasets that have been scraped from the Internet could pose safety risks. The authors should describe how they avoided releasing unsafe images.
    - We recognize that providing effective safeguards is challenging, and many papers do not require this, but we encourage authors to take this into account and make a best faith effort.

12. **Licenses for existing assets**

    Question: Are the creators or original owners of assets (e.g., code, data, models), used in the paper, properly credited and are the license and terms of use explicitly mentioned and properly respected?

    Answer: [Yes]

    Justification: Our method is evaluated on several datasets. We followed their license and we have credited and cited their work and datasets.

    Guidelines:

    - The answer NA means that the paper does not use existing assets.
    - The authors should cite the original paper that produced the code package or dataset.
    - The authors should state which version of the asset is used and, if possible, include a URL.
    - The name of the license (e.g., CC-BY 4.0) should be included for each asset.

- For scraped data from a particular source (e.g., website), the copyright and terms of service of that source should be provided.
- If assets are released, the license, copyright information, and terms of use in the package should be provided. For popular datasets, `paperswithcode.com/datasets` has curated licenses for some datasets. Their licensing guide can help determine the license of a dataset.
- For existing datasets that are re-packaged, both the original license and the license of the derived asset (if it has changed) should be provided.
- If this information is not available online, the authors are encouraged to reach out to the asset's creators.

13. **New Assets**

    Question: Are new assets introduced in the paper well documented and is the documentation provided alongside the assets?

    Answer: [NA] .

    Justification: N/A.

    Guidelines:

    - The answer NA means that the paper does not release new assets.
    - Researchers should communicate the details of the dataset/code/model as part of their submissions via structured templates. This includes details about training, license, limitations, etc.
    - The paper should discuss whether and how consent was obtained from people whose asset is used.
    - At submission time, remember to anonymize your assets (if applicable). You can either create an anonymized URL or include an anonymized zip file.

14. **Crowdsourcing and Research with Human Subjects**

    Question: For crowdsourcing experiments and research with human subjects, does the paper include the full text of instructions given to participants and screenshots, if applicable, as well as details about compensation (if any)?

    Answer: [NA]

    Justification: N/A.

    Guidelines:

    - The answer NA means that the paper does not involve crowdsourcing nor research with human subjects.
    - Including this information in the supplemental material is fine, but if the main contribution of the paper involves human subjects, then as much detail as possible should be included in the main paper.
    - According to the NeurIPS Code of Ethics, workers involved in data collection, curation, or other labor should be paid at least the minimum wage in the country of the data collector.

15. **Institutional Review Board (IRB) Approvals or Equivalent for Research with Human Subjects**

    Question: Does the paper describe potential risks incurred by study participants, whether such risks were disclosed to the subjects, and whether Institutional Review Board (IRB) approvals (or an equivalent approval/review based on the requirements of your country or institution) were obtained?

    Answer: [NA]

    Justification: N/A.

    Guidelines:

    - The answer NA means that the paper does not involve crowdsourcing nor research with human subjects.

- Depending on the country in which research is conducted, IRB approval (or equivalent) may be required for any human subjects research. If you obtained IRB approval, you should clearly state this in the paper.
- We recognize that the procedures for this may vary significantly between institutions and locations, and we expect authors to adhere to the NeurIPS Code of Ethics and the guidelines for their institution.
- For initial submissions, do not include any information that would break anonymity (if applicable), such as the institution conducting the review.